INTERNATIONAL SCIENTIFIC JOURNAL
GEOGRAPHICA PANNONICA
Volume 29, Issue 2, 84–107 (June 2025)
Journal homepage: http://www.dgt.uns.ac.rs/en/homepage/pannonica/

Fine-scale Mapping of Heat-hazard Risk and Vulnerability Using Geo-spatial Techniques: Insights from a Tropical Indian City

Rajashree Kotharkar[A*], Aveek Ghosh[A], Ravindra Keskar[A]

[A] *Visvesvaraya National Institute of Technology (VNIT), Nagpur, Maharashtra, India; ORCID RK: 0000-0002-5063-2757; AG: 0000-0002-5025-395X; RK: 0000-0002-3674-6539*

KEYWORDS

- extreme heat
- heat-hazard risk
- heat vulnerability index
- sensitivity
- exposure
- adaptive capacity
- local climate zone

ABSTRACT

Unprecedented extreme heat events (EHEs) have amplified associated health risks, but they present great differences within the urban environment. This paper aims to assess heat-hazard risk (HHR) and associated vulnerability in Nagpur, a heat-prone Indian city using remotely sensed and on-site meteorological data. HHR was generated through high resolution local climate zone (LCZ) maps via the product of hazard and vulnerability which featured census-tract socio-economic variables (sensitivity and adaptive capacity) and exposure. Principal component analysis (PCA) with equal weighting was applied to develop a composite fine-scale heat vulnerability index (HVI). Out of 136 wards, a total of 68 wards were identified to have 'high' or 'very high' HVI featuring about 49.06% of the population. LCZ-based spatial mapping showed a heterogeneous heat 'risk-scape' across the city. 'High' and 'very high' heat vulnerability/risk (HV/R) signature was observed in city core, its adjoining areas (LCZs 3 and 3_F) and urban fringes (LCZs 9 and 9_3). Conversely, open areas with moderate vegetation cover and natural classes (LCZs 6, 6B, A and B) showed 'moderate' to 'low' HHR. The findings of this research will enable the urban practitioners and policymakers to deal with explicit determinants of heat vulnerability and risk especially in regions with low adaptive capacity.

Introduction

Heat-related hazards pose major health risks in cities (Santamouris, 2019; Ebi et al., 2021) and significantly affect urban livability (Wouters et al., 2017; Kotharkar et al., 2024a, 2024b). Extreme heat events (EHEs) or heat waves (HWs), characterized as extended durations of abnormally elevated temperatures particularly result in excessive mortality rates (Gasparrini and Armstrong, 2011; Kumar & Singh, 2021). In recent past, multiple cities globally have suffered the brunt of frequent HWs including 2015 Indian and Pakistani HW (Wehner et al., 2016), 2016 South-East Asian HW (Gu et al., 2016), 2019 European HW (Pascal et al., 2021), 2020 Siberian HW (WMO, 2021) and 2021 North American HW (Keith et al., 2021). Multiple reports have predicted EHEs to be more intense, more frequent and longer-lasting, particularly in urbanized environments (IPCC, 2018, 2021). In this context, it is of paramount importance for urban practitioners to gain knowledge on heat vulnerability and associated socio-economic risks to manage and cope with EHEs.

* Corresponding author:Rajashree Kotharkar; e-mail: rskotharkar@gmail.com

doi: 10.5937/gp29-56164

Received: January 20, 2025| Revised: April 28, 2025| Accepted: May 22, 2025

In the recent past, multiple studies have conducted HV/R assessment across cities/metropolitan areas/regions with improving spatial accuracy (Maragno et al., 2020; Karanja et al., 2022). In this study, we define HV/R as a tool which can developed to identify the population or geographies that are at high risk of heat hazard (HH) using spatial socio-economic, physical and environmental data that are associated with heat-related adverse health outcomes. The external event of a HH can be referred to a dangerous condition or risk to public health caused by extreme heat episodes. This can result from high environmental temperatures, prolonged exposure to heat sources, or physical exertion in hot conditions. The knowledge of HV/R can subsequently inform urban planning policies, public health interventions, emergency measures and mitigation strategies. The wide range of studies shows concentration of research efforts in developed countries especially with tropical climates (Azhar et al., 2017; Hu et al., 2017; Rathi et al., 2021; Kotharkar et al., 2019; Li et al., 2022). Similarly, a number of research efforts have concentrated on mapping heat-health risks to evaluate intra-urban differences (Navarro-Estupiñan et al., 2020; Kotharkar & Ghosh, 2021a, 2021b; Zhou et al., 2021; Chen et al., 2022; Cheval et al., 2022; Ellena et al., 2023; Ma et al., 2023).

Urban environments exhibit significant variations in heat risks (HRs) and/or HHRs due to differences in surface morphologies and physical structures. In this paper, we define HHR as the potential harm to human health across population groups, due to exposure to extreme heat conditions in a given geographical area. To better understand the impact of different urban surfaces, Stewart and Oke (2012) introduced the concept of local climate zones (LCZs). LCZs are defined as the regions that possess similar characteristics like surface cover, material, structure, and population activity, extending from several hundred meters to a few kilometers. The framework has been extensively used to collect urban data by logically dividing the urban landscape (Lehnert et al., 2021). It has found its application in the wider assessment of heat-health risks in multiple cities (Verdonck et al., 2018; Chen et al., 2021), including Chongqing (Cai et al., 2019), Hermosillo (Navarro-Estupiñan et al., 2020), Beijing (Zhou et al., 2021; Chen et al., 2022), Turin (Ellena et al., 2023) and Changzhou (Ma et al., 2023). The wide range of assessments using spatial classification systems (e.g., LCZ maps) provides valuable input and decision support for climate adaptation planning to mitigate urban HRs. Such assessments can inform, guide and strengthen heat-health action plans (HHAPs) via extreme heat planning and management. A HHAP lays a strong foundation and serve as an effective tool for directing heat-related adaptation and mitigation efforts across spatial scales (Kotharkar & Ghosh 2021b). HHAPs aims to provide a methodical framework inclusive of public health responses, activation of alert systems and inter-agency coordination to reduce the negative impact of HWs. Hence, evidence-based local assessment of HV/R is crucial for augmenting the overall response to growing risks of HWs.

A widely used framework for assessing heat-related health risks is the 'Crichton Risk Triangle', which consists of three key components: hazard, exposure, and vulnerability (Crichton, 1999). Over the past decade, an increasing number of studies have adopted this framework for evaluating heat-related health risks (Hu et al., 2017; Estoque et al., 2020). With the advancement of research on LCZ, many studies have demonstrated that the framework is a valuable tool for analyzing various aspects of the urban thermal environment (Verdonck et al., 2018). For instance, Zhou et al. (2021) applied the LCZ system to examine heat risk in Beijing, specifically analyzing the distribution of LCZ types in relation to population heat exposure. Most previous studies assess risk at the level of administrative units (such as cities or neighborhoods) primarily due to data constraints. However, it lacks the resolution to capture the heterogeneous spatial distribution of populations within those boundaries. While such studies provide valuable insights for urban planning and management, they fall short in analyzing finer-scale relationships with urban structure, limiting their usefulness for implementing targeted planning measures (Hu et al., 2017; Zuhra et al., 2019; Chen et al., 2022). Additionally, past research has largely concentrated on heat-related hazards, with comparatively little attention given to exposure and vulnerability, which represents two critical components that shape the overall impact of hazards (Ren et al., 2022; Wu et al., 2022).

Research gap, novelty and significance of the study

The existing literature shows that the geographical distribution of HV/R assessments in Asian tropics as well as high population and development density settings (e.g., India) are not usually well known and remain less explored barring a few (Rathi et al., 2021; Shih & Mabon, 2021; Nanda et al., 2022; Ghosh et al., 2024). Moreover, due to limited availability of dense weather station data in these regions, several studies have used remotely-sensed land surface temperature (LST) to measure HH (Romero-Lankao et al., 2012). While some studies have highlighted that the UHI effect increases the extent and intensity of extreme heat stress in cities, most have focused solely on daytime temperatures, neglecting nighttime temperatures and potentially underestimating the overall HHR in urban areas. Research has shown that integrating heat exposure data with population vulnerability factors can effectively map high-risk areas and guide targeted interventions (Inostroza et al., 2016; Hu et al., 2017). Additionally, spatial frameworks enable the identification of heat risk hotspots from local to regional levels, supporting more effective climate adaptation planning and emergency management (Aubrecht & Özceylan, 2013; Ma et

al., 2023). As EHEs are predicted to increase in frequency and severity due to climate change, these spatial vulnerability assessments become increasingly important for developing targeted heatwave preparedness plans and reducing heat-related health risks (Ghosh, 2024). Hence, spatial vulnerability and risk estimation are crucial for understanding and mitigating heat-related hazards in urban areas (Karanja & Kiage, 2021; Li et al., 2022, 2024).

It has also been shown that LCZs vary in the levels of human thermal stress they experience due to extreme heat (Kotharkar et al., 2021, 2022). A study in Nagpur highlighted pedestrian discomfort and thermal stress in commercial streets, affecting walkability and public transit usage (Mohite & Surawar, 2024). Another research identified relatively high levels of thermal stress benchmarks with respect to respondent's sensation, comfort, tolerance and acceptability in Nagpur city (Kotharkar et al., 2024a). A recent comprehensive study by Kotharkar et al. (2024b) indicate that large low-rise, sparsely built, and scattered areas mixed with compact low-rise zones (i.e., LCZs 8, 9 and 9_3) present higher levels of heat stress indicating greater susceptibility to mortality. The wide variety of scientific literature constructs a possibility of different LCZs demonstrating variation in heat-related risks and implications. However, vulnerability-based research to inform extreme heat-related risks are still limited. LCZs with distinct surface morphologies and physical structures can help identify differences in HRs and provide a foundation for developing effective adaptation and mitigation strategies (Kotharkar et al., 2024c). This study uses the LCZ framework to standardize urban zones, a widely adopted method for examining spatio-temporal variations in the thermal environment. Therefore, to fill this research gap, the research conducts a comprehensive HV/R assessment combined with LCZ maps to provide valuable insights of high-risk areas at a local level with finer resolution.

The present study is first of its kind to employ a novel and hybrid approach to calculate HHR using census and local climate information (daytime and nighttime hazard analysis) in Nagpur, a heat-prone central Indian city. It attempts to spatially analyse and conduct a comprehensive heat-related health risk assessment using LCZ classification at a spatially explicit raster level. This is particularly critical in tropical and sub-tropical regions with limited adaptation solutions, low socioeconomic status and poor heat-health governance. These investigations can play a crucial role in mitigating the adverse impacts of HHs on households via easier implementation, thereby enhancing the urban thermal environment in cities.

Aim and objectives of the study

The present study aims to estimate HHR for Nagpur, a centrally located tropical Indian city. It attempts to assess local-level heat-health risk (HHR) using the LCZ classification to help inform and support decisions for the effective implementation of preventive measures in heat-health action plans (HHAPs). The objective of this paper is to explore the interaction of HH and related vulnerability at ward level. Mapping of HV involved estimating the spatial patterns of exposure, sensitivity and adaptive capacity using principal component analysis (PCA) tool and identifying the influencing variables.

Study area and climate

Nagpur (21.1458° N, 79.0882° E; 310 meters above sea level) is a tropical city located in central India. The city, administered by the municipal corporation, has a population of approximately 2.4 million and a gross population density of 110 people per hectare (pph) (MHA, 2011). Spanning an area of 217.65 km², Nagpur is the 13th largest city in India by population. The city is relatively compact, with dense core areas. In the peripheral regions, particularly in the western and southwestern parts, the population density ranges from 20 to 32 pph, while in the inner and core areas, the density can reach as high as 750 to 1,000 pph. Nine wards situated in the city center has density in the

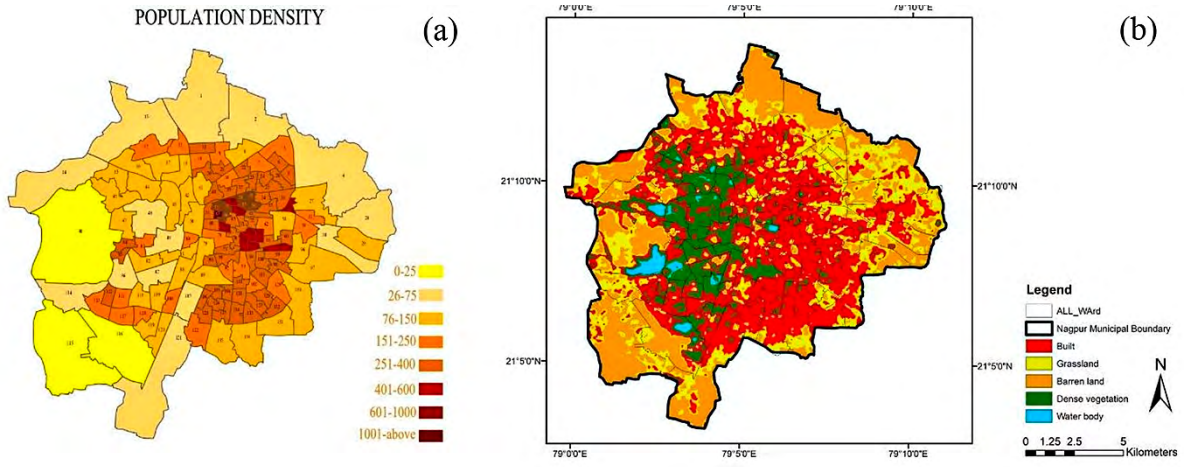

Figure 1 a, b. Population density of Nagpur city in 2011 (b) LULC map

range of 601–1000 pph while ward no. 67 has population density in excess of 1000 pph (refer Fig. 1a). In 2021, area covered under built-up, grassland, vegetation (sparse and dense), barren and water bodies were 41.2%, 12.13%, 17.31 %, 26.07% and 3.29%, respectively (see Fig. 1b). Slums are spread over an area of 17 km^2 (7.81%) while >2% of the land is officially classified as urban green spaces.

The city has a tropical savanna climate, classified as "Aw" under the Köppen climate system. It experiences four distinct seasons: summer (March to June), monsoon (July to August), post-monsoon (September to October), and winter (November to February). Historically, annual temperatures range from a record high of 48°C during summer to a low of 4°C during winter (Kotharkar et al., 2021). However, city's tropical climate experiences significant temperature variations throughout the year. Summers are exceptionally hot, often accompanied by frequent heatwave days, locally known as *'loo'*. In recent past, the city has witnessed record extreme temperatures coupled with recurrent HWs with increasing intensities. These extreme summer conditions create uncomfortable outdoor environments and pose exacerbated thermal discomfort.

Materials and methods

The HHR mapping workflow is carried out in four stages, as shown in Figure 2. The present research was aided by various software including ArcGIS v10.4, Autodesk AutoCAD v2020, HOBOware v3.7.4, MS Excel v2011, and statistical software 'R' v4.2.1. The stages of the study can be described as:

1. The first stage involved a literature review of previous HV/R assessments across geographic locations and climate zones to identify appropriate indicators which are best possible fit. The indicators from each variable to describe vulnerability were extracted from 2011 census data, which was pre-processed (conversion from vector to raster form) and normalized for further analysis. Simultaneously, LCZ mapping of Nagpur city was conducted using WUDAPT technique (Bechtel et al., 2015; Mills et al., 2015). To estimate HH, in-situ air temperature measurements (refer Fig. 3) were carried out across different LCZs covering major parts of the city.
2. In the second stage, PCA with varimax rotation was used as a dimension reduction technique to filter the actual indicators explaining majority of the variance. The HVI scores (ward-wise) were normalized on a scale of 0 to 1.

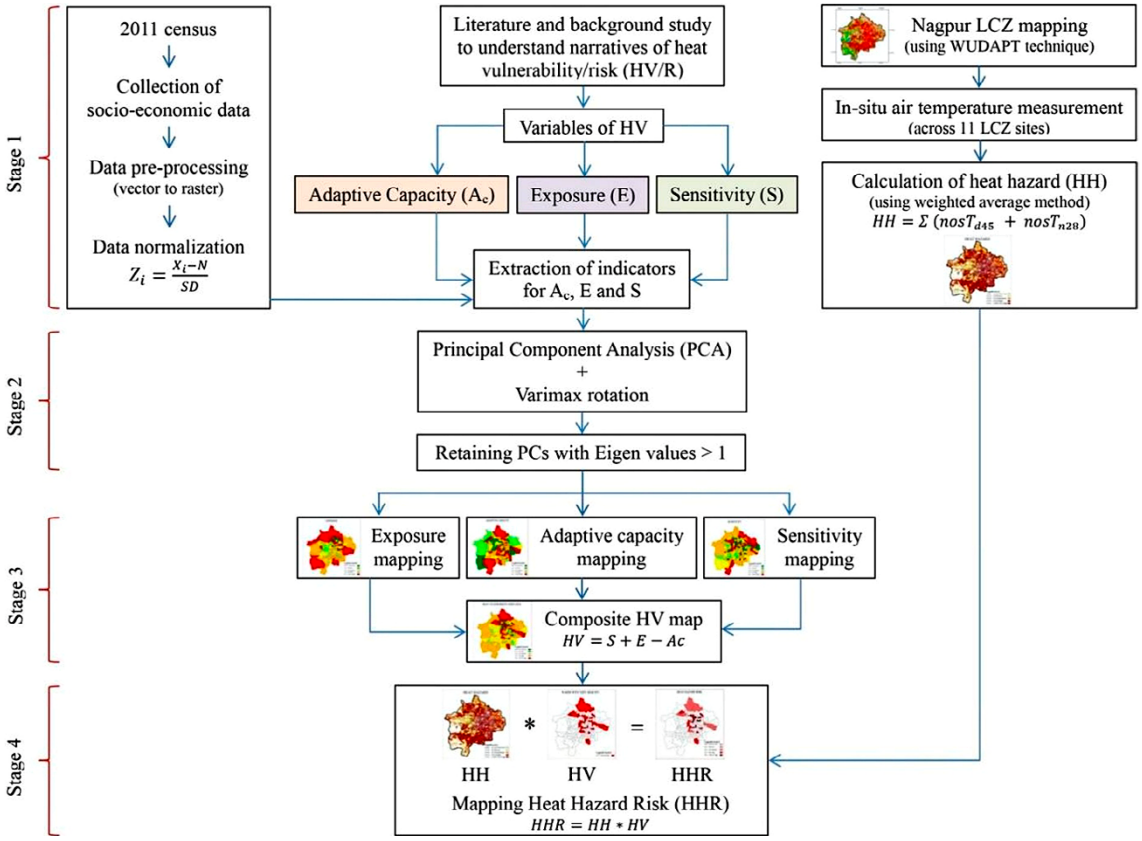

Figure 2. Workflow for HHR mapping

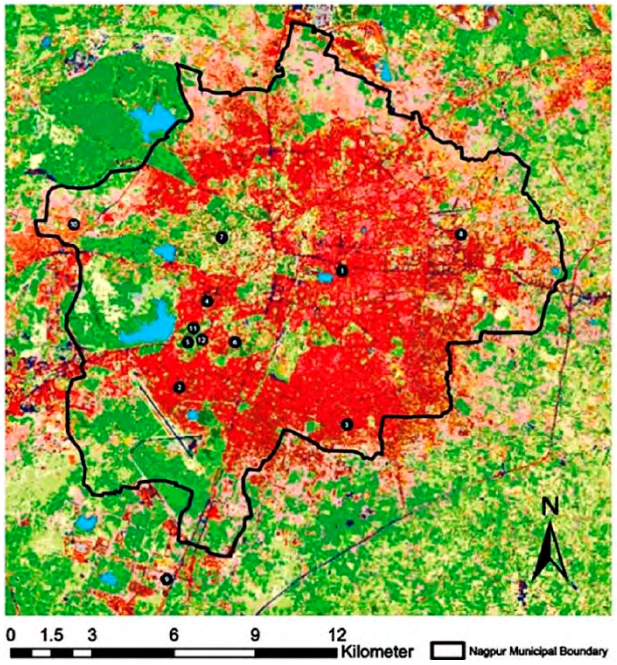

Sr	Area	Description
1	MHL LCZ 3	Densely built compact low-rise area with scarce vegetation and abundance of impervious surfaces
2	DDN LCZ 3_F	Low-rise built forms with moderately low amount of vegetation and bare soil
3	MNW LCZ 3_F	Low-rise and compact urban setting with high coverage of bare surfaces and low amount of vegetation
4	SVJN LCZ 5	Open area with midrise buildings, and moderate pervious surface
5	VNIT LCZ 6	Open low-rise blocks with abundance of vegetation and pervious surfaces
6	BJN LCZ 6_S	Mix of low-rise and mid-rise built forms with moderate amount of vegetation
7	ADT LCZ 6_B	Open low rise blocks with abundance of pervious land cover and vegetation
8	APMC LCZ 8	Large open low-rise area with moderate amount of paved surface
9	Khapri LCZ 9	Sparsely built low-rise setting with scarce vegetation and abundance of pervious surfaces
10	DBA LCZ 9_3	Sparsely built low-rise setting nested with few compact low-rise buildings
11	VNIT A LCZ A	Area with dense vegetation and wooded trees
12	VNIT Park LCZ B	Area with scattered trees, pavements and patches of grasslands

Two stations representative of LCZ 3_F were selected as the city showed a high coverage of the same

Figure 3. LCZ map of Nagpur city showing measurement locations

3. The third stage encompassed spatial mapping of HV variables (adaptive capacity, exposure and sensitivity) which led to the generation of composite HV map using eqn. 2. Wards with very high HVI as well as dominant LCZs were identified and spatial overlap and the intensity of HHR across LCZ classes were analyzed.
4. The fourth and the final stage involved the estimation of HHR using the product of HH and HV (for wards with very high HV).

HV assessment

The census at municipal ward level, developed by the Office of the Registrar General and Census Commissioner of India, Ministry of Home Affairs, Government of India was used for spatial analysis. The 2011 census data within continuous urban area of Nagpur municipality (consisting 136 wards) was obtained from https://censusindia.gov.in/census.website/data/census-tables. A composite heat vulnerability index (HVI) was developed using spatially explicit variables of sensitivity, adaptive capacity and exposure. Duplicate variables that represented similar constructs were removed and diverse indicators across demographic, social, economic, health, and environmental domains were selected. The present study encompasses a combined total of twenty-one (21) indicators including eight (8) indicators of adaptive capacity, twelve (12) indicators for sensitivity and LST as the sole indicator for exposure (refer Annexure I). It considers that HVI is triggered by sensitivity and exposure and diminished with increasing adaptive capacity (see eqn. 1 and 2), which can be represented as:

$$\text{Heat Vulnerability} = f\ (\text{Exposure, Sensitivity, Adaptive capacity}) \quad (1)$$

This can be mathematically calculated as shown in eqn. 2:

$$HV = S + E - A_c \quad (2)$$

where, HV is the composite heat vulnerability, S refers to sensitivity level, E refers to exposure level, and A corresponds to the adaptive capacity.

Adaptive Capacity

Adaptive capacity denotes the residents' capability to respond to the adverse impacts of extreme heat and rebound from any resulting losses. Eight indicators constituted adaptive capacity which included access to infrastructure and other coping mechanisms (electricity, water, communication/health/social facilities, personal vehicle and bank account) which help residents to survive periods of extreme heat (Kovats & Hajat, 2008) (see Annexure I). NDVI was included as an indicator reflecting higher proportion of vegetation and its health which reduces heat intensity (Raja et al., 2021).

Sensitivity

'Sensitivity' is the degree to which urban population is affected by heat-related stimuli (IPCC, 2014; Sharma & Ravindranath, 2019). Twelve (12) indicators obtained from census data were deduced to determine sensitivity (see Annexure I). This include illiterate population and person with disability as they are not aware of the negative effects of extreme heat (Cutter et al., 2003; Uejio et al., 2011; Raja et al.,

2021) and possess fewer resources to combat the heat exposure and thus are vulnerable to heat stress. Females, young children (below 6 years) and elderly (above 60 years) population were accounted as they are susceptible to EHEs (Wilhelmi & Hayden, 2010; Nayak et al., 2018). It also included the socioeconomically marginalized section (scheduled caste and scheduled tribes). It further considered population density, typology of dwelling units, average number of inhabitants per household and single household sizes to account for sensitive population groups.

Exposure

'Exposure' to extreme heat is referred to as the external impact of HH on the population. In the present study, exposure is represented by LST, which is considered to be one of the most influential variables to describe heat exposure (Zuhra et al., 2019), which heightens extreme heat issues (Reid et al., 2009; Aubrecht & Özceylan, 2013).

Heat-hazard estimation

HH is captured through the intensity and distribution of extreme heat. The study accounted for the nocturnal effect by integrating Tmax with daily minimum temperature (T_{min}). T_{max} and T_{min} across selected LCZs were used to represent HWs and hot nights respectively to account for its intensity and frequency. The study applied the HW criteria formulated by the India Meteorological Department (NDMA, 2019) for the plains of India. HW conditions are identified when the maximum temperature at a station reaches 45°C or higher during the day. HH was calculated by summing the instances when the daily maximum temperature exceeded 45°C during daytime ($nosT_{d45}$) and/or 28°C during nighttime ($nosT_{n28}$). These daily instances were then aggregated and normalized to create an HH index. (see eqn. 3):

$$HH = \frac{\sum\left(nosT_{d45} + nosT_{n28}\right)}{\text{Total instances}} \quad (3)$$

where, HH is the heat hazard, $nosT_{d45}$ refers to number of days with daily maximum temperature above 45°C, and $nosT_{n28}$ is the number of days with daily minimum temperature above 28°C. The total instances were estimated to be 108 (54 days * 2 instances for each day reflecting daytime and nighttime condition). The daytime conditions were considered during 06:00 – 17:59 hrs while nighttime conditions denoted 18:00 – 05:59 hrs.

A threshold 28°C was selected as an indicator of tropical night which is often used to measure extreme high nighttime temperature (nocturnal discomfort). However, the selection of threshold for indicating tropical nights is inconsistent in the scientific literature. Nocturnal thermal high is considered when T_{min} exceeding an absolute threshold such as 25-28°C or 90% or 95% percentile of its climatological series (Ha & Yun, 2012; Klok et al., 2023). The present study selected the threshold (28°C) based on the research conducted in similar tropical Asian countries (Korea and South China) (Chen et al., 2023; Klok et al., 2023).

Local climate zone mapping and collection of summertime air temperature

The LCZ mapping of Nagpur city employed the World Urban Database and Access Portal Tools (WUDAPT) method (Bechtel et al., 2015) to process remotely sensed images using ArcGIS 10.4.4. Pixel-based classification techniques for LCZ mapping have become widely used in urban areas (Verdonck et al., 2017; La et al., 2020). Each pixel was assigned to a single LCZ, and the remotely sensed data was cropped to the region of interest, defined by the Nagpur municipal boundary. The vector processing and supervised classification process involved selecting LCZ training areas from Google Earth, based on expert knowledge. LANDSAT 8 data was then used, along with the maximum likelihood classification (MLC) tool, to classify the LCZs. This process was repeated iteratively until an accurate LCZ map was produced.

Stationary surveys were conducted during the summer of 2022 to gather data across various LCZs (see Figure 2). These sites, representing urban areas with distinct microclimates, provided a 54-day dataset for analysis. The locations were chosen based on LCZ mapping covering ~ 75% area of Nagpur city. Measurements of T_{air} were taken at an elevation between 1.5 - 2 meters above ground level, and recorded at five-minute intervals. Days with abnormal and missing values were filtered. The final dataset was used for further assessment. The instrument setup featured a built-in temperature sensor housed in a radi-

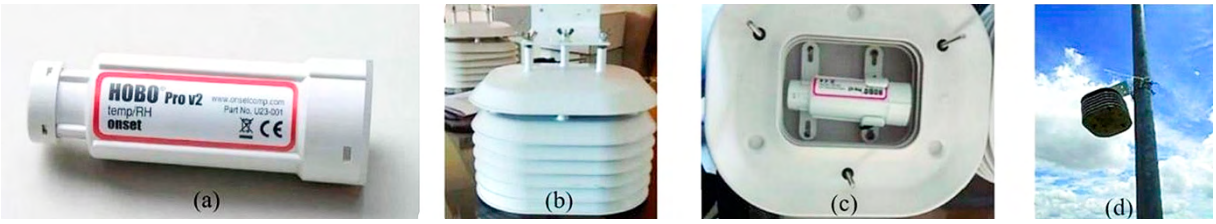

Figure 4. (a) HOBO pro V2 data logger (b) Radiation shield (c) Data logger placed inside the shield (d) Instrument placed at site

ation shield. An Onset HOBO U-23 Pro V2 weatherproof data logger, accurate to ±0.2°C within a temperature range of 0–70°C, was used for data collection (refer Fig. 4a-d). All necessary precautions and specifications were followed during the surveys (Oke, 2004; Runnalls & Oke, 2006).

Heat-hazard risk assessment

The study employed Crichton's conceptual definition of the risk triangle (Crichton, 1999) and IPCC AR4 (IPCC, 2007) to develop the HHR map. This notion offers a concise structure overlapping the layers of hazard and vulnerability. Multiple studies have demonstrated that the multiplicative principle accurately captures the intricate interaction between hazard and vulnerability (Estoque et al., 2020). The present study adopted the methodology used by Ma et al. (2023) and estimated the combined HHR as the aggregate of hazard and vulnerability (refer eqn. 4), which can be understood as:

$$HHR = HH \cdot HV \tag{4}$$

where, *HHR* is the heat-hazard risk, *HH* refers to heat hazard, and *HV* denotes heat vulnerability.

The allocation of weights to indices within the risk triangle framework has been a point of inconsistency in prior literature (Reckien, 2018). Therefore, this study opts for assigning equal weights to the layers of hazard and vulnerability in generating the *HHR*.

Statistical analysis

PCA was applied to embrace multiple factors of vulnerability (Wolf & McGregor, 2013; Inostroza et al., 2016; Nayak et al., 2018; Kotharkar et al., 2019). This approach has proven reliable as a method for reducing dimensions, creating independent principal components (PCs) that accurately represent the maximum variance. A composite PC score (z-score) was formulated to indicate the statistical deviation from the mean value (Wolf & McGregor, 2013). The variance-weighted approach (Schmidtlein et al., 2008) was applied, with the ranking of principal components (PCs) based on the amount of data variability they capture. This ranking is represented by the eigenvalues associated with the vector of each PC (Inostroza et al., 2016). The Pearson correlation matrix was used to observe relationship of individual variables. The variables was standardised as PCA is highly dependent on input vaules. This was accomplished by transforming the values into z-scores (utilizing eqn. 5):

$$Z_i = \frac{X_i - N}{SD} \tag{5}$$

where, Z_i represents the z-score for each ward, X_i denotes the original value, N signifies the mean of all indicator values, and SD represents the standard deviation of the individual indicator values.

The adequacy of the data for PCA was evaluated using the Kaiser-Meyer-Olkin (KMO) test and Bartlett's test of sphericity. For sampling adequacy, the KMO estimate should be more than 0.50 (on a scale from 0 to 1) and *p value <0.001* to pass Bartlett's test (Adnan et al., 2023). The Kaiser eigenvalue criterion (eigenvalue > 1) was employed along with orthogonal varimax rotation to extract PCs as suggested by Kaiser (1960). Varimax rotation was chosen due to its capability to extract highly independent components (Raja et al., 2021). Any component that accounted for approximately 10% of the variance, or where the cumulative percent of the retained components was at least 70%, was kept. The calculated scores from Eqn. (2) were integrated to compute the aggregated HVI score. Subsequently, Eqn. (6) was applied to standardize the HVI scores for each ward on a scale from 0 to 1 (Inostroza et al., 2016):

$$\beta = \left[\frac{x - x_{min}}{x_{max} - x_{min}} \right] \tag{6}$$

where, β represents the normalized HVI value for each ward, while x denotes the original HVI value. The terms x_{min} and x_{max} refer to the lowest and highest HVI values, respectively.

The HVI was calculated by summing the scores from each component for each ward. These normalized HVI values were then grouped into five categories—'very low', 'low', 'moderate', 'high', and 'very high'—based on the GIS methodology outlined by Raja et al. (2021).

Estimation of satellite-based LST and NDVI

The study utilized the Thermal Infrared Sensor (TIRS) and Operational Land Imager (OLI) instruments of LANDSAT 8 to acquire daytime Land Surface Temperature (LST) data. [imagery date: 22 April 2022; cloud cover: 2.97%; sun elevation: 66°; (path 144, row 45)], which overlaps with the period of data collection across LCZ sites (year 2022). The date was selected as it represents a typical hot summer day for Nagpur city. Satellite imagery for Nagpur was obtained from open-source data (https://eos.com/landviewer/?lat=21.14510&lng=79.08610&z=11). LANDSAT 8 satellite data offer several advantages, including enhanced radiometric and spectral resolution, a better signal-to-noise ratio, refined bandwidth, and two thermal infrared bands (Dube & Mutanga 2015; Karlson et al. 2015). LST was extracted by widely adopted methodology in multiple studies (Zanter, 2016; Navarro-Estupiñan; 2020).

Results and findings

The present study evaluated city-scale HH and related vulnerability to estimate HHR for Nagpur city. The findings are presented in four sub-sections which include; a) spatial distribution of LST, NDVI and LCZ classes (b) constructing a composite HVI using the indicators of adaptive capacity, sensitivity and exposure (c) mapping of HH and HHR.

Spatial distribution of LCZ classes and mapping of LST and NDVI

The LCZ mapping of Nagpur city showed a heterogeneous and uneven structure and confirmed its compact pattern (refer Fig. 5a). It has 10 built types (LCZs 1-10) and zones with few nested LCZs (LCZs 3_7, 3_F, 6_5, 6_B and 9_3). Built and natural types accounted for 72.61% and 27.39% area respectively (refer Fig. 5b). The central regions were primarily characterized by a combination of compact low-rise settings (LCZ 3) and mid-rise buildings (LCZ 2). In contrast, the peripheral areas were dominated by LCZs 9 and 9_3. LCZ 6_5 (open mid-rise nested in open low-rise zone) constitutes a significant sub-class among built zones, accounting for approximately 9.97% of the total area. LCZs 3 and 9 were the dominant zones covering 14.74% and 9.86% of the area respectively (refer Fig. 5c).

The city center comprising LCZs 3 (38.78°C) and 3_7 (38.99°C) showed lower LST_{max} values mainly due to mutual shading attributed to densely packed buildings (see Fig. 5d). Outer city limits embracing LCZs 9 (max. 41.78°C) and 9_3 (max. 41.02°C) generally showed higher LST_{max} values due to high daytime exposure. LCZs 3_F (max. 40.03°C) and F (max. 46.69°C) also showed higher values due to the presence of bare patches. Areas with lower temperatures were predominantly concentrated in water bodies and vegetated areas. These regions have the capacity to moderate temperatures through mechanisms such as heat absorption, evapotranspiration, and shading. The average LST observed for built-up areas was 35.05°C, while for vegetation it was 33.59°C, and for water bodies, it stood at 26.85°C.

The spatial pattern of Land Surface Temperature (LST) aligns with the distribution of LCZs, where areas with a higher concentration of built-up zones tend to exhibit higher LST values (refer Fig. 3d). An average LST of 35.58°C was observed while the maximum and minimum values were 53.23°C and 17.94°C respectively. The peripheral areas especially along the northern, south-western zones were characterized by higher LST values. Spatial differences in NDVI showed lack of greenness/vegetation within the city limits (refer Fig. 5e). Core areas comprising high density settings showed lower NDVI values. The pixel-based maximum and minimum NDVI values were observed to be 0.435 and -0.101 respectively. There is a notable negative correlation observed LST and NDVI, indicated by a Pearson correlation coefficient of -0.354 ($p<0.01$), suggesting a statistically significant relationship between the two variables.

Developing a composite HVI

In the next step, the Pearson correlation matrix was calculated to assess the strength and direction of the relationship between the two variables. Indicators of adaptive capacity when correlated with those of sensitivity, yielded moderate to strong relationships (see Table 1). For instance, electricity supply was positively correlated with population density (+0.48), housing typology (+0.559) and single household size (+0.648). NDVI was negatively correlated with roof material (-0.229) and LST (-0.354). Indicators of sensitivity were found to be strongly correlated with infrastructural facilities (e.g., water/electricity supply, access to communication). Communication facilities (access to landline/mobile) showed a strong positive relationship with building typology (+0.804), single household size (+0.647), average number of people/household (+0.665) and rented housing (+0.632). LST as the sole indicator of exposure was found to be positively associated with building typology (+0.407), population density (+0.496) and roof material (0.551).

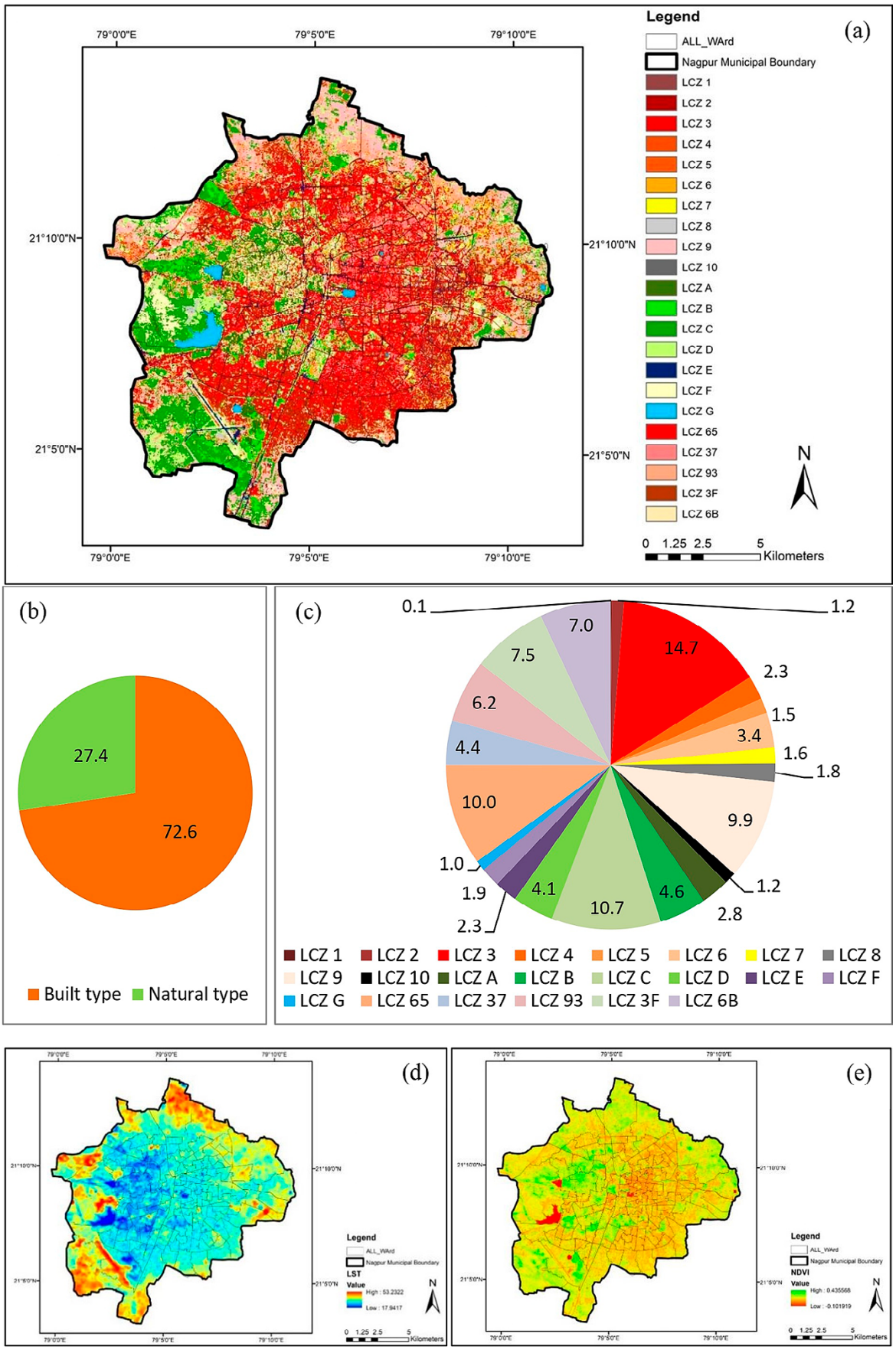

Figure 5. (a) LCZ mapping of Nagpur city (b) proportion of built and natural types (c) overall coverage of different LCZs (d) Pixel-based mapping of LST (e) spatial distribution of NDVI

Table 1. Correlation matrix (Pearson)

Indicators	ES	WS	CF	HF	SF	PV	BA	NDVI	IP	FP	YP	OP	SCST	PD	POP	TYP	SH	HH	RH	TS	RM	DIS	LST
ES	**1**	0.144	**0.492**	**0.449**	**0.593**	0.177	0.296	0.052	**0.423**	-0.095	-0.078	-0.399	0.145	**0.480**	0.170	**0.559**	**0.648**	0.392	**0.741**	**0.573**	**0.730**	-0.051	0.242
WS	0.144	**1**	0.143	0.130	-0.046	-0.128	**0.501**	-0.157	0.055	0.281	-0.084	0.296	-0.053	-0.083	-0.091	0.181	0.114	-0.013	0.106	-0.197	0.133	0.209	-0.12
CF	**0.492**	0.143	**1**	**0.856**	**0.496**	**0.518**	0.288	-0.027	**0.677**	0.287	-0.250	-0.275	0.139	-0.123	**-0.441**	**0.804**	**0.647**	**0.665**	**0.632**	0.126	-0.171	0.377	0.29
HF	**0.449**	0.130	**0.856**	**1**	0.365	**0.460**	0.308	0.184	**0.703**	0.401	-0.054	-0.287	0.025	-0.073	-0.308	**0.896**	**0.754**	**0.673**	**0.717**	0.355	**0.791**	**0.508**	-0.116
SF	**0.593**	-0.046	**0.496**	0.365	**1**	0.106	-0.078	0.096	**0.473**	-0.149	-0.094	-0.113	0.066	0.301	-0.099	**0.447**	**0.514**	**0.553**	**0.657**	**0.703**	**0.571**	0.025	0.087
PV	0.177	-0.128	**0.518**	**0.460**	0.106	**1**	-0.044	-0.162	**0.491**	0.059	-0.183	-0.089	0.156	-0.297	-0.283	**0.477**	0.299	0.273	0.266	0.326	0.396	0.032	0.085
BA	0.296	0.501	0.288	0.308	-0.078	-0.044	**1**	0.035	0.196	0.197	-0.334	0.000	-0.018	0.200	0.092	0.262	0.283	0.045	0.268	-0.233	0.244	-0.112	-0.178
NDVI	0.052	-0.157	-0.027	0.184	0.096	-0.162	0.035	**1**	0.014	-0.292	-0.171	0.037	0.168	-0.39	-0.289	**-0.408**	0.219	0.132	-0.261	-0.14	-0.229	-0.35	-0.354
IP	**0.423**	0.055	**0.677**	**0.703**	**0.473**	**0.491**	0.196	0.014	**1**	0.142	-0.368	-0.240	0.239	0.161	-0.123	**0.730**	**0.693**	**0.535**	**0.749**	**0.601**	**0.749**	-0.296	0.039
FP	-0.095	0.281	0.287	0.401	-0.149	0.059	0.197	-0.292	0.142	**1**	-0.125	0.134	**-0.442**	-0.259	-0.365	**0.445**	0.404	0.056	0.266	-0.067	0.227	-0.365	0.008
YP	-0.078	-0.084	-0.250	-0.054	-0.094	-0.183	-0.334	-0.171	-0.368	-0.125	**1**	-0.121	-0.166	0.062	0.015	-0.173	-0.140	-0.020	-0.106	-0.053	-0.057	-0.268	-0.057
OP	-0.399	0.296	-0.275	-0.287	-0.113	-0.089	0.000	0.037	-0.240	0.134	-0.121	**1**	-0.188	-0.294	-0.215	-0.271	-0.336	-0.259	-0.401	-0.361	-0.376	0.021	0.131
SCST	0.145	-0.053	0.139	0.025	0.066	0.156	-0.018	0.168	0.239	**-0.442**	-0.166	-0.188	**1**	0.008	0.004	-0.110	-0.188	0.221	-0.134	0.062	-0.051	0.103	-0.06
PD	**0.480**	-0.083	-0.123	-0.073	0.301	-0.297	0.200	-0.39	0.161	-0.259	0.062	-0.294	0.008	**1**	**0.654**	-0.001	0.193	0.190	0.376	0.291	0.370	**0.424**	**0.496**
POP	0.170	-0.091	**-0.441**	-0.308	-0.099	-0.283	0.092	-0.289	-0.123	-0.365	0.015	-0.215	0.004	**0.654**	**1**	-0.222	-0.117	-0.158	-0.022	-0.115	0.141	**0.516**	0.204
TYP	**0.559**	0.181	**0.804**	**0.896**	**0.447**	**0.477**	0.262	**-0.408**	**0.730**	**0.445**	-0.173	-0.271	-0.110	-0.001	-0.222	**1**	**0.916**	**0.500**	**0.843**	**0.508**	**0.877**	0.038	**0.407**
SH	**0.648**	0.114	**0.647**	**0.754**	**0.514**	0.299	0.283	0.219	**0.693**	0.404	-0.140	-0.336	-0.188	0.193	-0.117	**0.916**	**1**	0.314	**0.947**	**0.555**	**0.853**	-0.257	-0.175
HH	0.392	-0.013	**0.665**	**0.673**	**0.553**	0.273	0.045	0.132	**0.535**	0.056	-0.020	-0.259	0.221	0.190	-0.158	**0.500**	0.314	**1**	**0.458**	**0.510**	**0.608**	0.031	0.289
RH	**0.741**	0.106	**0.632**	**0.717**	**0.657**	0.266	0.268	-0.261	**0.749**	0.266	-0.106	-0.401	-0.134	0.376	-0.022	**0.843**	**0.947**	**0.458**	**1**	**0.689**	**0.909**	-0.274	0.23
TS	**0.573**	-0.197	0.126	0.355	**0.703**	0.326	-0.233	-0.14	**0.601**	-0.067	-0.053	-0.361	0.062	0.291	-0.115	**0.508**	**0.555**	**0.510**	**0.689**	**1**	**0.628**	0.119	-0.172
RM	**0.730**	0.133	-0.171	0.791	**0.571**	0.396	0.244	-0.229	**0.749**	0.227	-0.057	-0.376	0.051	0.370	0.141	**0.877**	**0.853**	**0.608**	**0.909**	**0.628**	**1**	0.07	**0.551**
DIS	-0.051	0.209	0.377	0.508	0.025	0.032	-0.112	-0.35	-0.296	-0.365	-0.268	0.021	0.103	**0.424**	**0.516**	0.038	-0.257	0.031	-0.274	0.119	0.07	**1**	-0.08
LST	0.242	-0.12	0.29	-0.116	0.087	0.085	-0.178	-0.354	0.039	0.008	-0.057	0.131	-0.06	**0.496**	0.204	**0.407**	-0.175	0.289	0.23	-0.172	**0.551**	-0.08	**1**

Values in bold present strong statistical relationship at a significance level alpha=0.05

A composite HVI was derived by aggregating the components with equal weight and then normalizing the result. The PCA yielded consistent outcomes with nearly constant values for the eigenvalues and loadings of PCs, as depicted in Table 4. The present study estimated KMO values in the range of 0.59-0.73 and *p-value* to be 2.2e-16 (see Table 2) which taken together proves the suitability of dataset for HV analysis.

Table 2. Measure of Kaiser-Meyer-Olkin (KMO) and Bartlett's test of sphericity

Adaptive Capacity		Sensitivity		Exposure	
KMO	Bartlett's p-value	KMO	Bartlett's p-value	KMO	Bartlett's p-value
0.73	2.2e-16	0.59	2.2e-16	0.62	2.2e-16

The results of PCA highlighted the respective contributions of various factors to the HVI (refer Table 3). Two PCs with eigenvalues > 1 collectively explained 71.38% of the variance in the dataset (PC1: 44.02% and PC2: 27.36%). According to the rotated component matrices, PC1 was mainly presented indicators of adaptive capacity which included communication facilities (-0.270), health facilities (+0.719) and sensitivity indicators comprising female population (+0.537), young population (+0.692), population density (+0.753), average number of people/household (+0.679) and roof material (+0.610). PC2 mainly featured other indicators of sensitivity illiterate population (+0.730), elderly population (+0.628), SC/ST population (+0.531) and LST (+0.520). The PC loadings indicated that infrastructural facilities act as coping solutions while demographic factors and housing conditions are major influencing indicators of HV.

The HV mapping was generated using its composite values (see Annexure II). Subsequent mapping of HV variables showed distinct variation across different wards of the city. Administrative wards in core areas showed a greater

Table 3. PC loadings for indicators

	Indicators	PC1	PC2	PC3	PC4	PC5	PC6
ADPATIVE CAPACITY	1. Electricity supply	+0.106	-0.007	+0.112	+0.032	+0.014	+0.005
	2. Water supply	+0.087	+0.806^	-0.040	+0.223	-0.020	+0.119
	3. Communication facilities	-0.270*	+0.051	+0.140	-0.051	+0.117	-0.02
	4. Health facilities	+0.719*	+0.023	+0.198	+0.157	+0.039	-0.024
	5. Social facilities: religious facilities & schools	-0.091	+0.044	-0.069	+0.56	+0.063	-0.223
	6. Personal vehicle	-0.183	+0.102	-0.027	+0.009	+0.066	-0.006
	7. Bank account	-0.113	+0.039	-0.005	-0.142	-0.096	+0.081
	8. Normalized Difference Vegetation Index	-0.234	+0.017	+0.184	-0.058	+0.104	-0.026
SENSITIVITY	9. Illiterate Population	+0.101	+0.730^	-0.146	+0.087	+0.04	+0.097
	10. Female population	+0.537*	+0.014	+0.060	+0.161	-0.126	-0.015
	11. Population aged under 6 years	+0.692*	+0.056	+0.139	+0.042	-0.003	+0.008
	12. Population aged over 60 years	+0.173	+0.628^	+0.409	+0.006	-0.144	-0.101
	13. Population of Scheduled Caste (SC)/ Scheduled Tribe (ST)	+0.060	+0.531^	-0.071	-0.018	+0.068	-0.09
	14. Population density	+0.753*	+0.181	+0.048	+0.039	-0.032	+0.142
	15. Typology of houses	+0.056	-0.109	+0.486	+0.072	+0.194	+0.055
	16. Single household size	+0.480	+0.504	+0.094	+0.091	+0.043	-0.027
	17. Average number of people per household	+0.679*	+0.091	+0.003	-0.006	-0.018	-0.031
	18. Rented housing	-0.131	+0.128	+0.152	+0.153	+0.039	+0.077
	19. Roof material	+0.610*	+0.103	-0.018	+0.068	-0.018	-0.165
	20. Population that has disability 18-64 years	-0.058	+0.158	+0.031	+0.024	+0.058	-0.084
EXPOSURE	21. Land surface temperature	+0.18	+0.520	+0.029	+0.082	-0.045	-0.02

*Note: Statistically significant ones are values > 0.5; * Statistically significant values for PC1; ^ Statistically significant values for PC2*

mix of 'very low' and 'very high' adaptive capacity. Core areas mostly represent a mix of old neighborhoods and newly developed zones. This may possibly be attributed to a difference in infrastructural facilities (water and electricity supply), urban redevelopment initiatives and presence of differential vegetation cover. Such moderations can cause change in adaptive capacity within core areas. Urban fringes in western direction had lower levels. Adaptive capacity was generally 'very high' in the wards located in far northern and southern fringes. The core and adjoining areas generally showed 'moderate and 'high' levels of exposure while majority of fringes featured in 'very high' levels. The results revealed that more than 66% of the area was in 'high' or 'very high' exposure range. For sensitivity, western fringes were found to be in 'high' range while core areas generally showed 'moderate' values. About 40% of the area was found to be with 'very low' and 'low' sensitivity levels (refer Fig. 6).

els and 24.54% were located in 'moderate' level. 33 wards in 'very high' levels of HV were used for further analysis to calculate HHR. These were mainly located towards the eastern side and distributed in the city center and fringes. A detailed assessment of HV mapping revealed that a total of 69 wards present with 'high' (0.31-0.41) and 'very high' (>0.41) HVI. A total area of 39.7 km^2 (out of total 217.65 km^2) in the city was found to have 'high' and 'very high' HVI but constituted 49.06% of the population (about 1.18 million). Majority of the 'high' and 'very high' HV areas were dominated by compact low-rise neighbourhoods, sparsely-built settings and built areas nested with bare soil.

Mapping of HH and HHR

Mapping of HH accounted for the intensity and frequency of HW event during the 2022 summer season. The hazard map revealed the distribution of high temperature days (both daytime and nighttime above a certain threshold)

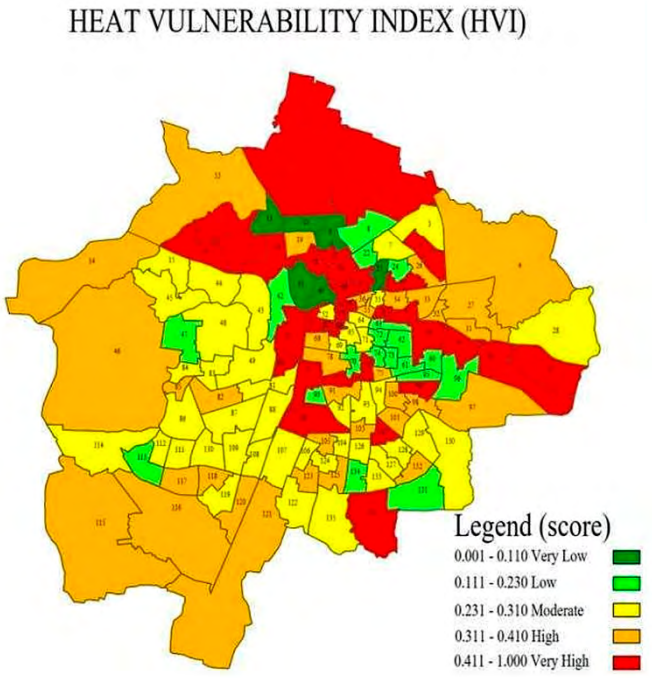

Figure 6. Spatial extent and distribution of HVI

The HV mapping was generated using eqn. (2) using its composite values 'Very high' levels of HV were found in core and urban fringes. Areas with moderate vegetation cover correspond to 'low' or 'very low' HV while most of the residential areas featured in 'moderate' level. The mapping showed a greater variation in the eastern direction while the western fringes majorly presented a consistent HV signature in 'moderate' level. The composite HV map showed a distribution of 'very low' in 5 wards; 'low' in 20 wards; 'moderate' in 42 wards; 'high' in 36 wards while 33 wards were under 'very high' category. About one-fourth of the population was found to be in 'very low' or 'low' levbased on on-site data collection across different LCZs (see Fig. 7a). Mapping results revealed that a high percentage (>50%) of land area is exposed to 'very high' HH. Majority of 'very high' HH areas were found to be concentrated in the central, eastern and southern parts of the city. Among the built classes, HH levels were found to be 'very high' for LCZs 3 (0.481), 3_F (0.472), 5 (0.426), 6_5 (0.444), 8 (0.454) and 9_3 (0.481) as they experienced high daytime and nocturnal heat stress. 'High' HH was observed for LCZ 6 (0.352) while LCZ 9 showed 'moderate' value (0.306). Open zones with vegetation/trees (LCZ 6_B) and natural classes (LCZs A and B) demonstrated 'low' HH values. Fringe areas in

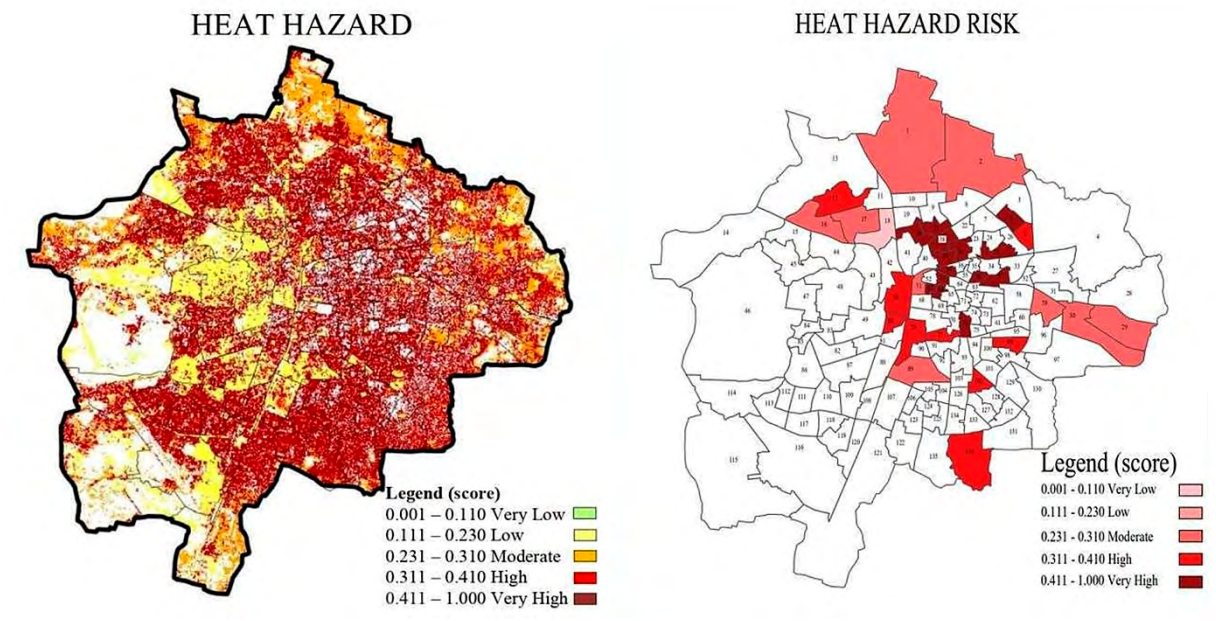

Figure 7. Spatial distribution of (a) heat hazard (b) heat hazard risk

the north-eastern direction generally showed 'moderate' HH values. The spatial distribution of HHR for wards with 'very high' HV is shown in Fig. 7 (b). HHR in the city centre of Nagpur appears to be higher compared to the suburbs. Out of the 33 wards with 'very high' HV, 14 wards were designated with 'very high' HHR (>0.411) and were located in the east-central part of the city. These constitute highly dense areas coupled with very high population density. 'High' (9 wards) and 'moderate' (9 wards) HHR constituted 18 wards and were distributed across the core areas and urban fringes.

LCZ-based HHR mapping revealed that densely built areas generally had higher values. LCZs constituting at least 75% of the wards were extracted and termed as 'dominant' ones. Due to differences in urban morphology that LCZs represent, their corresponding risk levels were found to be varied (see table 4). Spatial overlap and the intensity of heat risk across LCZ classes were analysed for 33 wards which featured with 'very high' composite HVI scores. The intersection of wards and HHR distribution mostly aligns (commonly prevalent) for LCZs 3, 3F and 9. In a few wards, there exists disagreements. 'Very high' HHR were characteristic for LCZ 3 and 3_F while 'high' HHR values corresponded for LCZs 3, 3_7, 3_F, 6_5 and 9. Natural (LCZs A and B) and built classes with vegetation cover (LCZ 6_B) showed 'moderate' and/or 'low' HHR. 'Very high' and 'high' HHR areas covered 17.43 km^2, accounting for about 8% of the total area. This shows a great deal of spatial heterogeneity in HHR even within wards with 'very high' HV. The findings reflect that compact low-rise and its variants (LCZs 3 and 3_F) and sparsely built zones and its variants (LCZ 9 and 9_3) agree with the distribution of HHR across these administrative wards. Conversely, LCZ classes (3_7, 6, 6_5, 6_B and B) disagree when wards and HHR values intersect.

Table 4. Prevalent LCZs with very high HVI and respective HHR

Ward No	HVI score	Dominant LCZs	Heat Hazard Risk (level)
1	0.483	3 & 9	0.291 (moderate)
2	0.511	3 & 9	0.294 (moderate)
5	0.616	3, 3_7 & 9	0.401 (high)
6	0.547	3_7 & 9_3	0.577 (very high)
12	0.493	3 & 6_5	0.399 (high)
16	0.441	3 & 6_5	0.305 (moderate)
17	0.529	3, 5, & 9	0.254 (moderate)
18	0.477	3, 6_5, & 6_B	0.108 (very low)
20	0.532	3 & 6	0.452 (very high)
21	0.45	3 & 9_3	0.592 (very high)
25	0.474	3 & 3_F	0.532 (very high)
29	0.776	3 & 9	0.309 (moderate)
30	0.797	3, 6 & 9	0.263 (moderate)
37	0.573	3 & 3_F	0.451 (very high)
38	0.541	3 & 3_F	0.510 (very high)
39	0.42	3	0.492 (very high)
50	0.56	3, & 6_B	0.359 (high)
51	0.444	3, 6, & 3_F	0.282 (moderate)
53	0.423	3	0.542 (very high)
54	0.479	3	0.531 (very high)
56	0.724	3	0.617 (very high)
57	0.579	3, 6 & 3_F	0.516 (very high)
59	0.495	3, 6 & 9	0.310 (moderate)
66	0.522	3	0.555 (very high)
67	0.447	3	0.618 (very high)
76	0.448	3	0.491 (very high)
77	0.428	3, 3_F & B	0.401 (high)
79	0.444	3, 6, & 6_B	0.399 (high)
80	0.416	3 & 9_3	0.352 (high)
89	0.437	3, 6, & 6_B	0.246 (moderate)
99	0.42	3, 3F, & 6_5	0.356 (high)
102	0.416	3, 6 & 3_F	0.359 (high)
136	0.642	3, 9 & 3_F	0.380 (high)

Discussion

The present study carried out a comprehensive HV/R assessment for Nagpur, a tropical and heat-prone Indian city. The city experiences extreme summertime conditions and often witness severe HW conditions, thus affecting a large and sprawling city (Mohite & Surawar, 2024). Research efforts in Nagpur have demonstrated a strong correlation between heat stress indices and all-cause mortality, with certain LCZ classes showing higher susceptibility to heat stress (Kotharkar et al., 2024a; Dutta et al., 2020). The aim was to pinpoint populations or geographic areas at elevated risk by leveraging spatial socio-economic and environmental data. PCA was utilized to assess vulnerability encompassing three underlying vulnerability components: exposure, sensitivity, and adaptive capacity. Among the indicators of adaptive capacity, infrastructural facilities (such as access to water, electricity, mobile/landline services, healthcare/social facilities, and NDVI) showed a negative correlation with HVI. Such findings

corroborate the results of previous studies (Rinner et al., 2010; Adnan et al., 2023). Social isolation was found to be another risk factor (Luber & McGeehin 2008, Uejio et al., 2011). PCA generated two PCs where the first one consisted of infrastructural facilities, specific population groups (young and females) and housing characteristics while the other one featured LST, illiterate, elderly, and SC/ST population (Cutter et al., 2003; Azhar et al., 2017; Karanja et al., 2025). Health care services provided by medical infrastructure (e.g., hospitals, clinics) were identified as crucial indicators. Education level was found to be associated with socio-economic status, as high illiteracy rates indicate a reduced ability to read and understand heat-health warnings.

Spatial distribution of HV revealed three clusters with 'very high' values. These wards, characterized by high population density, are scattered across the central part of the city and are represented by older neighbourhoods and core residential areas. This distribution aligns with the outcomes reported in previous studies (Wolf & McGregor, 2013; Raja et al., 2021). The study found LCZs 8 and 10 to be associated with higher LST but with relatively low risk similar to the findings in Changzhou, China (Ma et al., 2023). This is due to low population density as against other residential and compact zones (LCZs 3 and 3_F) (Ma et al., 2023). It proves that LST is not a good indicator for HH assessment. Additionally, differential adaptive capacity was observed within core areas owing to demographic shifts, urban redevelopment and changes in infrastructural facilities. The study also confirmed a significant negative correlation between LST and NDVI which provides strong scientific evidence for increasing urban green spaces for effective heat mitigation.

The Pearson correlation matrix revealed a statistically significant positive relationship between overall heat vulnerability and lack of adaptive capacity, aligning with the findings of Rathi et al. (2021) and Hess et al. (2012). Previous studies describe the relationship between adaptive capacity and vulnerability in three ways: (1) they are not mutually exclusive, (2) vulnerability can result from limited adaptive capacity along with other factors, and (3) they are inversely related, meaning greater adaptive capacity leads to lower vulnerability and vice versa (Brooks et al., 2005; Gaillard, 2010). In this study, vulnerability was found to be directly proportional to the lack of adaptive capacity. This suggests that municipal authorities should implement short-term measures to improve the adaptive capacity of vulnerable households, while also developing long-term strategies to reduce their exposure and sensitivity.

The present study found significant variation in HHR levels across different LCZs. It also noted that compact low-rise zones and its variants (LCZs 3 and 3_F) occupying a large proportion of area showed 'high' and 'very high' HHR. This could be attributed to closely spaced buildings coupled with minimal vegetation leading to less evapotranspiration (Li et al., 2025; Zou et al., 2025). Additionally, these zones have a high percentage of impervious surfaces with densely built areas representative of older urban neighbourhoods or inner-city residential zones. These zones reflect a higher population density and anthropogenic heat release which require urgent attention. Conversely, midrise LCZs (LCZs 2 and 5) did not exhibit high risk. This could be due a combination of factors related to urban morphology, and socioeconomic context. These zones house less vulnerable populations owing to better infrastructure facilities (water and electricity). The findings align with previous empirical evidence observed in hot-dry tropical/sub-tropical climates (Huang et al., 2023) and other cities in China (Cai et al., 2019; Li et al., 2022). Peripheral areas representative of LCZs 9 and 9_3 also featured with 'very high' HHR. Conversely, low-density and open developments (LCZ 6 and 6_B) presented lesser risks to extreme heat (Inostroza et al., 2016). Previous studies on high density and heterogeneous developments also support similar findings (Zhou et al., 2021; Chen et al., 2022; Cheval et al., 2022). These findings align with past research in Nagpur city which has shown an increasing trend in maximum temperatures, and hot nights, with heat stress indices rising over time (Kotharkar et al., 2024b).

The limitations of the study need to be acknowledged. Firstly, the present research used 2011 census data to estimate HV, as the 2021 census was postponed due to the COVID-19 pandemic. This may create some discrepancy among data collection dates and inevitably result in some temporal ambiguity in the index estimates. Secondly, ward-wise mortality data was unavailable which limits the validity of HV estimation. Lastly, equal weightage was allotted to the indicators which may not represent unique characteristics of cities. Weightings can be adjusted based on new insights into heat-related health issues or specific user needs. Future studies can include multiple instances represented by several LST imagery can enhance the accuracy and reliability of HV. Additionally, research efforts can account for biometeorological indices to better quantify the exposure.

Conclusion

Urban heat and extended periods of hot weather present a significant challenge to residents and cause heat-related health risks. The present study assessed HHR and estimated associated vulnerability using the variables of adaptive capacity, sensitivity and exposure. It used a detailed, granular approach, incorporating both remotely sensed

and on-site meteorological data to estimate the city-level HHR. The mapping of heat vulnerability revealed significant spatial asymmetry in its distribution. City centres and adjoining areas along with urban fringes were recognized with 'very high' HHR while open developments and areas with moderate vegetation cover presented lesser HRs. The HHR map for Nagpur serves as an effective tool for devising heat mitigation strategies and identifying hotspot areas, aiding in the identification of vulnerable zones or populations. This approach aids in identifying risk prevention strategies and prioritizing heat management tactics at the municipal level. Application of spatial frameworks (e.g., LCZ map used in this study) could provide crucial insights for urban planners to consider climate-based recommendations to alleviate extreme heat in specific zones in a city. The results could inform evidence-based guidelines within city-level HHAPs.

Researchers agree that urban HV/R is a complex phenomenon characterized by significant spatial and temporal variability. As a result, HV/R assessments must be dynamic, adapting to recognize evolving risks driven by changes in urban characteristics. Future research efforts could be extended to the implementation of a localized heat early warning system and can be conducted in cities which are likely to be affected by future warming. Future research could consider supplementary indicators, such as pre-existing medical or chronic conditions, access to air conditioning, income level, and other relevant data. In addition, enhancing the quality of LCZ as a spatial unit of analysis can improve the overall interpretation of results. The methodology adopted in the present study with slight adjustments can act as a guide for an accurate retrieval of HHR and allows for greater replicability across different spatial scales.

Acknowledgement

The study is under the research project "Developing framework for heat vulnerability mapping and model heat action plan for Indian cities", supported by the National Disaster Management Authority (NDMA), New Delhi, Government of India (Sanction No. 1-111/2019-PP). We thank the Department of Architecture & Planning, Visvesvaraya National Institute of Technology (VNIT), Nagpur for providing the necessary infrastructure.

References

Adnan, M. S. G., Kabir, I., Hossain, M. A., Enan, M. S., Chakma, S., Tasneem, S. N., Hassan, Q. K., & Dewan, A. (2023). Heatwave vulnerability of large metropolitans in Bangladesh: an evaluation. *Natural Hazards*. (preprint version). https://doi.org/10.21203/rs.3.rs-3093933/v1

Aubrecht, C., & Özceylan, D. (2013). Identification of heat risk patterns in the U.S. National Capital Region by integrating heat stress and related vulnerability. *Environment International*, 56, 65–77. 10.1016/j.envint.2013.03.005

Azhar, G., Saha, S., Ganguly, P., Mavalankar, D., & Madrigano, J. (2017). Heat Wave Vulnerability Mapping for India. *International Journal of Environmental Research and Public Health*, 14(4), 357. 10.3390/ijerph14040357

Bechtel, B., Alexander, P., Böhner, J., Ching, J., Conrad, O., Feddema, J., ... & Stewart, I. (2015). Mapping Local Climate Zones for a Worldwide Database of the Form and Function of Cities. *ISPRS International Journal of Geo-Information*, 4(1), 199–219. 10.3390/ijgi4010199

Brooks, N., Adger, W. N., & Kelly, P. M. (2005). The determinants of vulnerability and adaptive capacity at the national level and the implications for adaptation. *Global environmental change*, 15(2), 151-163. https://doi.org/10.1016/j.gloenvcha.2004.12.006

Cai, Z., Tang, Y., Chen, K., & Han, G. (2019). Assessing the Heat Vulnerability of Different Local Climate Zones in the Old Areas of a Chinese Megacity. *Sustainability*, 11(7), 2032. https://doi.org/10.3390/su11072032

Chen, B., Xie, M., Feng, Q., Wu, R., & Jinag, L. (2022). Diurnal heat exposure risk mapping and related governance zoning: A case study of Beijing, China. *Sustainable Cities and Society*, 81, 103831. https://doi.org/10.1016/j.scs.2022.103831

Chen, R., Wen, Z., Lin, W., & Qiao, Y. (2023). Diverse relationship between the tropical night in South China and the water vapor transport over the South China Sea and the plausible causes. *Atmospheric Research*, 296, 107080. https://doi.org/10.1016/j.atmosres.2023.107080

Chen, T-L., Lin, H., & Chiu, Y-H. (2021). Heat vulnerability and extreme heat risk at the metropolitan scale: A case study of Taipei metropolitan area, Taiwan. *Urban Climate*, 41, 101054. https://doi.org/10.1016/j.uclim.2021.101054

Cheval, S., Dumitrescu, A., Amihăesei, V., Irașoc, A., Paraschiv, M.-G., & Ghent, D. (2022). A country scale assessment of the heat hazard-risk in urban areas. *Building and Environment*, 229, 109892. https://doi.org/10.1016/j.buildenv.2022.109892

Crichton, D. (1999) The Risk Triangle. In: Ingleton, J., Ed., *Natural Disaster Management*, Tudor Rose, London, 102-103.

Cutter, S. L., Boruff, B. J., & Shirley, W. L. (2003). Social vulnerability to environmental hazards. *Social Science Quarterly*, 84(1), 242–261. https://doi.org/10.1111/1540-6237.8402002

Dube, T., & Mutanga, O. (2015). Evaluating the utility of the medium-spatial resolution Landsat 8 multispectral sensor in quantifying aboveground biomass in uMgeni catchment, South Africa. *ISPRS Journal of Photogrammetry and Remote Sensing*, 101, 36–46. https://doi.org/10.1016/j.isprsjprs.2014.11.001

Dutta, P., Sathish, L., Mavankar, D., Ganguly, P. S., & Saunik, S. (2020). Extreme Heat Kills Even in Very Hot Cities: Evidence from Nagpur, India. *The international journal of occupational and environmental medicine*, 11(4), 188–195. https://doi.org/10.34172/ijoem.2020.1991

Ebi, K. L., Capon, A., Berry, P., Broderick, C., de Dear, R., Havenith, G., ... & Jay, O. (2021). Hot weather and heat extremes: health risks. *The Lancet*, 398(10301), 698–708. https://doi.org/10.1016/S0140-6736(21)01208-3

Ellena, M., Melis, G., Zengarini, N., Di Gangi, E., Ricciardi, G., Mercogliano, P., & Costa, G. (2023). Micro-scale UHI risk assessment on the heat-health nexus within cities by looking at socio-economic factors and built environment characteristics: The Turin case study (Italy). *Urban Climate*, 49, 101514. https://doi.org/10.1016/j.uclim.2023.101514

Estoque, R. C., Ooba, M., Seposo, X. T., Togawa, T., Hijioka, Y., Takahashi, K., & Nakamura, S. (2020). Heat health risk assessment in Philippine cities using remotely sensed data and social-ecological indicators. *Nature Communications*, 11(1). https://doi.org/10.1038/s41467-020-15218-8

Gaillard, J. C. (2010). Vulnerability, capacity and resilience: Perspectives for climate and development policy. *Journal of International Development: The Journal of the Development Studies Association*, 22(2), 218-232. https://doi.org/10.1002/jid.1675

Gasparrini, A., & Armstrong, B. (2011). The impact of heat waves on mortality. *Epidemiology (Cambridge, Mass.)*, 22(1), 68–73. https://doi.org/10.1097/EDE.0b013e3181fdcd99

Ghosh, A. (2024). Smart Heat-health Action Plans: A programmatic, progressive and dynamic framework to address urban overheating. *Geographica Pannonica*, 28(3), 221-237. https://doi.org/10.5937/gp28-51694

Gu, S., Huang, C., Bai, L., Chu, C., & Liu, Q. (2016). Heat-related illness in China, summer of 2013. *International Journal of Biometeorology*, 60(1), 131–137. 10.1007/s00484-015-1011-0

Ha, K. J., & Yun, K. S. (2012). Climate change effects on tropical night days in Seoul, Korea. *Theoretical and applied climatology*, 109, 191-203. https://doi.org/10.1007/s00704-011-0573-y

Hess, J. J., McDowell, J. Z., & Luber, G. (2012). Integrating climate change adaptation into public health practice: using adaptive management to increase adaptive capacity and build resilience. *Environmental health perspectives*, 120(2), 171–179. https://doi.org/10.1289/ehp.1103515

Huang, H., Ma, J., & Yang, Y. (2023). Spatial heterogeneity of driving factors for urban heat health risk in Chongqing, China: A new identification method and proposal of planning response framework. *Ecological Indicators*, 153, 110449. https://doi.org/10.1016/j.ecolind.2023.110449

Hu, K., Yang, X., Zhong, J., Fei, F., & Qi, J. (2017). Spatially Explicit Mapping of Heat Health Risk Utilizing Environmental and Socioeconomic Data. *Environmental Science and Technology*, 51(3), 1498–1507. 10.1021/acs.est.6b04355

Inostroza, L., Palme, M., & de la Barrera, F. (2016). A Heat Vulnerability Index: Spatial Patterns of Exposure, Sensitivity and Adaptive Capacity for Santiago de Chile. PLOS ONE, 11(9), e0162464. https://doi.org/10.1371/journal.pone.0162464

IPCC. (2007). *Summary for policymakers.* In M. L. Parry, O. F. Canziani, J. P. Palutikof, P. J. van der Linden, & C. E. Hanson (Eds.), *Climate change 2007: Impacts, adaptation and vulnerability. Contribution of Working Group II to the Fourth Assessment Report of the Intergovernmental Panel on Climate Change* (pp. 7–22). Cambridge University Press.

IPCC. (2014). *Summary for policymakers.* In C. B. Field, V. R. Barros, D. J. Dokken, K. J. Mach, M. D. Mastrandrea, T. E. Bilir, ... L. L. White (Eds.), *Climate change 2014: Impacts, adaptation, and vulnerability. Part A: Global and sectoral aspects. Contribution of Working Group II to the Fifth Assessment Report of the Intergovernmental Panel on Climate Change* (pp. 1–32). Cambridge University Press.

IPCC. (2018). *Global warming of 1.5°C: An IPCC special report on the impacts of global warming of 1.5°C above pre-industrial levels and related global greenhouse gas emission pathways, in the context of strengthening the global response to the threat of climate change, sustainable development, and efforts to eradicate poverty* (V. Masson-Delmotte, P. Zhai, H.-O. Pörtner, D. Roberts, J. Skea, P. R. Shukla, et al., Eds.). In press.

IPCC. (2021). *Summary for policymakers.* In V. Masson-Delmotte, P. Zhai, A. Pirani, S. L. Connors, C. Péan, S. Berger, N. Caud, Y. Chen, L. Goldfarb, M. I. Gomis, M. Huang, K. Leitzell, E. Lonnoy, J. B. R. Matthews, T. K. Maycock, T. Waterfield, O. Yelekçi, R. Yu, & B. Zhou (Eds.), *Climate change 2021: The physical science basis. Contribution of Working Group I to the Sixth Assessment Report of the Intergovernmental Panel on Climate Change.* Cambridge University Press. In press.

Kaiser, H. F. (1960). The application of electronic computers to factor analysis. *Educational and Psycho-*

logical Measurement, 20(1), 141–151. https://doi.org/10.1177/001316446002000116

Karanja, J., & Kiage, L. (2021). Perspectives on spatial representation of urban heat vulnerability. *Science of The Total Environment*, 774, 145634. https://doi.org/10.1016/j.scitotenv.2021.145634

Karanja, J., Vanos, J., Georgescu, M., Frazier, A. E., & Hondula, D. (2025). The Imperative for Hazard and Place-Specific Assessment of Heat Vulnerability. *Environmental health perspectives*. https://doi.org/10.1289/EHP14801

Karanja, J., Wanyama, D., & Kiage, L. (2022). Weighting mechanics and the spatial pattern of composite metrics of heat vulnerability in Atlanta, Georgia, USA. *Science of The Total Environment*, 812, 151432. https://doi.org/10.1016/j.scitotenv.2021.151432

Karlson, M., Ostwald, M., Reese, H., Sanou, J., Tankoano, B., & Mattsson, E. (2015). Mapping Tree Canopy Cover and Aboveground Biomass in Sudano-Sahelian Woodlands Using Landsat 8 and Random Forest. *Remote Sensing*, 7(8), 10017–10041. https://doi.org/10.3390/rs70810017

Keith, L., Meerow, S., Hondula, D. M., Turner, V. K., & Arnott, J. C. (2021). Deploy heat officers, policies and metrics. *Nature*, 598(7879), 29–31. https://doi.org/10.1038/d41586-021-02677-2

Klok, S., Kornus, A., Kornus, O., Danylchenko, O., & Skyba, O. (2023). Tropical nights (1976–2019) as an indicator of climate change in Ukraine. *IOP Conference Series: Earth and Environmental Science*, 1126(1), 012023. https://doi.org/10.1088/1755-1315/1126/1/012023

Kotharkar, R., Aneja, S., & Ghosh, A. (2019). Heat vulnerability index for urban heat wave risk adaptation for Indian cities: A case study of Akola. *5th International Conference on Countermeasures to Urban Heat Islands (IC2UHI), 02–04 December 2019, International Institute of Information Technology – Hyderabad, India*. https://doi.org/10.37285/bsp.ic2uhi.10

Kotharkar, R., Dongarsane, P., & Ghosh, A. (2024a). Quantification of summertime thermal stress and PET range in a tropical Indian city. *Urban Climate*, 53, 101758. https://doi.org/10.1016/j.uclim.2023.101758

Kotharkar, R., Dongarsane, P., Ghosh, A. & Kotharkar, V. (2024b). Numerical analysis of extreme heat in Nagpur city using heat stress indices, all-cause mortality and local climate zone classification. *Sustainable Cities and Society*, 101, 105099. https://doi.org/10.1016/j.scs.2023.105099

Kotharkar, R., & Ghosh, A. (2021a). Review of heat wave studies and related urban policies in South Asia. *Urban Climate*, 36, 100777. https://doi.org/10.1016/j.uclim.2021.100777

Kotharkar, R., & Ghosh, A. (2021b). Progress in extreme heat management and warning systems: A systematic review of heat-health action plans (1995-2020). *Sustainable Cities and Society*, 76, 103487. https://doi.org/10.1016/j.scs.2021.103487

Kotharkar, R., Ghosh, A., Kapoor, S., & Reddy, D. G. K. (2022). Approach to local climate zone based energy consumption assessment in an Indian city. *Energy & Buildings*, 259, 111835. https://doi.org/10.1016/j.enbuild.2022.111835

Kotharkar, R., Ghosh, A., & Kotharkar, V. (2021). Estimating summertime heat stress in a tropical Indian city using Local Climate Zone (LCZ) framework. *Urban Climate*, 36, 100784. https://doi.org/10.1016/j.uclim.2021.100784

Kotharkar, R., Vidyasagar, A., & Ghosh, A. (2024). Application of LCZ to urban heat island studies. In R. Wang, M. Cai, C. Ren, & Y. Shi (Eds.), *Local climate zone application in sustainable urban development* (pp. 79-103). Springer. https://doi.org/10.1007/978-3-031-56168-9_5

Kovats, R. S., & Hajat, S. (2008). Heat stress and public health: A critical review. *Annual Review of Public Health*, 29(1), 41–55. https://doi.org/10.1146/annurev.publhealth.29.020907.0908

Kumar, A., & Singh, D. P. (2021). Heat stroke-related deaths in India: An analysis of natural causes of deaths, associated with the regional heatwave. *Journal of Thermal Biology*, 95, 102792. 10.1016/j.jtherbio.2020.102792

La, Y., Bagan, H., & Yamagata, Y. (2020). Urban land cover mapping under the local climate zone scheme using Sentinel-2 and PALSAR-2 data. *Urban Climate*, 33, 100661. https://doi.org/10.1016/j.uclim.2020.100661

Lehnert, M., Savić, S., Milošević, D., Dunjić, J., & Geletič, J. (2021). Mapping Local Climate Zones and Their Applications in European Urban Environments: A Systematic Literature Review and Future Development Trends. *ISPRS International Journal of Geo-Information*, 10(4), 260. 10.3390/ijgi10040260

Li, F., Yigitcanlar, T., Li, W., Nepal, M., Nguyen, K., & Dur, F. (2024). Understanding urban heat vulnerability: Scientometric analysis of five decades of research. *Urban Climate*, 56, 102035. https://doi.org/10.1016/j.uclim.2024.102035

Li, F., Yigitcanlar, T., Nepal, M., Thanh, K., & Dur, F. (2022). Understanding Urban Heat Vulnerability Assessment Methods: A PRISMA Review. *Energies*, 15(19), 6998. http://dx.doi.org/10.3390/en15196998

Li, F., Yigitcanlar, T., Nepal, M., Nguyen, K., Dur, F., & Li, W. (2025). Mapping heat vulnerability in Australian capital cities: A machine learning and multi-source data analysis. *Sustainable Cities and Society*, 119, 106079. https://doi.org/10.1016/j.scs.2024.106079

Luber, G., & McGeehin, M. (2008). Climate change and extreme heat events. *American journal of preventive medicine*, 35(5), 429–435. https://doi.org/10.1016/j.amepre.2008.08.021

Ma, L., Huang, G., Johnson, B. A., Chen, Z., Li, M., Yan, Z., Zhan, W., Lu, H., Hw, W., & Lian, D. (2023). Inves-

tigating urban heat-related health risks based on local climate zones: A case study of Changzhou in China. *Sustainable Cities and Society*, 91, 104402. https://doi.org/10.1016/j.scs.2023.104402

Maragno, D., Dalla Fontana, M., & Musco, F. (2020). Mapping Heat Stress Vulnerability and Risk Assessment at the Neighborhood Scale to Drive Urban Adaptation Planning. *Sustainability*, 12, 1056. https://doi.org/10.3390/su12031056

Ministry of Home Affairs (MHA). (2011). Census of India, 2011. The Registrar General & Census Commissioner, Government of India. https://www.censusindia.gov.in/2011common/census_2011.html

Mills, G., Ching, J., See, L., Bechtel, B., & Foley, M. (2015). An introduction to the WUDAPT project. In *Proceedings of the 9th International Conference on Urban Climate* (pp. 20–24).

Mohite, S., & Surawar, M. (2024). Assessing pedestrian thermal comfort to improve walkability in the urban tropical environment of Nagpur city. *Geographica Pannonica*, 28(1). https://doi.org/10.5937/gp28-48166

Nanda, L., Chakraborty, S., Mishra, S. K., Dutta, A., & Rathi, S. K. (2022). Characteristics of Households' Vulnerability to Extreme Heat: An Analytical Cross-Sectional Study from India. *International journal of environmental research and public health*, 19(22), 15334. https://doi.org/10.3390/ijerph192215334

National Disaster Management Authority (NDMA). (2019). *National guidelines for preparation of action plan – Prevention and management of heat wave, 2019.* Ministry of Home Affairs, Government of India. https://ndma.gov.in

Navarro-Estupiñan, J., Robles-Morua, A., Díaz-Caravantes, R., & Vivoni, E. R. (2020). Heat risk mapping through spatial analysis of remotely-sensed data and socioeconomic vulnerability in Hermosillo, México. *Urban Climate*, 31, 100576. https://doi.org/10.1016/j.uclim.2019.100576

Nayak, S. G., Shrestha, S., Kinney, P. L., Ross, Z., Sheridan, S. C., Pantea, C. I., ... & Hwang, S. A. (2018). Development of a heat vulnerability index for New York State. *Public Health*, 161, 127–137. 10.1016/j.puhe.2017.09.006

Oke, T. R. (2004). *Initial guidance to obtain representative meteorological observations at urban sites* (IOM Report No. 81, WMO/TD-No. 1250, 47 pp.). World Meteorological Organization. https://www.wmo.int/pages/prog/www/IMOP/publications/IOM-81/IOM-81UrbanMetObs.pdf

Pascal, M., Lagarrigue, R., Tabai, A., Bonmarin, I., Camail, A., Laaidi, K., ... & Denys, S. (2021). Evolving heat waves characteristics challenge heat warning systems and prevention plans. *International Journal of Biometeorology*, 65, 1683–1694. https://doi.org/10.1007/s00484-021-02123-y

Raja, D. R., Hredoy, M. S. N., Islam, M. K., Islam, K. M. A., & Adnan, M. S. G. (2021). Spatial distribution of heatwave vulnerability in a coastal city of Bangladesh. *Environmental Challenges*, 4, 100122. https://doi.org/10.1016/j.envc.2021.100122

Rathi, S. K., Chakraborty, S., Mishra, S. K., Dutta, A., & Nanda, L. (2021). A Heat Vulnerability Index: Spatial Patterns of Exposure, Sensitivity and Adaptive Capacity for Urbanites of Four Cities of India. *International journal of environmental research and public health*, 19(1), 283. https://doi.org/10.3390/ijerph19010283

Reckien, D. (2018). What is in an index? Construction method, data metric, and weighting scheme determine the outcome of composite social vulnerability indices in New York City. Regional *Environmental Change*, 18(5), 1439–1451. 10.1007/s10113-017-1273-7

Reid, C., O'Neill, M., Gronlund, C., Brines, S., Brown, D., Diez-Roux, A., & Schwartz, J. (2009). Mapping Community Determinants of Heat Vulnerability. *Environmental Health Perspectives*, 117(1). 10.1289/ehp.0900683

Ren, J., Yang, J., Zhang, Y., Xiao, X., Xia, J. C., Li, X., & Wang, S. (2022). Exploring thermal comfort of urban buildings based on local climate zones. *Journal of Cleaner Production*, 340, 130744. https://doi.org/10.1016/j.jclepro.2022.130744

Rinner, C., Patychuk, D., Bassil, K., Nasr, S., Gower, S., & Campbell, M. (2010). The Role of Maps in Neighborhood-level Heat Vulnerability Assessment for the City of Toronto. Cartography and Geographic *Information Science*, 37(1), 31–44. 10.1559/152304010790588089

Romero-Lankao, P., Qin, H., & Dickinson, K. (2012). Urban vulnerability to temperature-related hazards: A meta-analysis and meta-knowledge approach. *Global Environmental Change*, 22(3), 670-683. 10.1016/j.gloenvcha.2012.04.002

Runnalls, K. E., & Oke, T. R. (2006). A Technique to Detect Microclimatic Inhomogeneities in Historical Records of Screen-Level Air Temperature. *Journal of Climate*, 19, 959–978. https://doi.org/10.1175/JCLI3663.1

Santamouris, M. (2019). Recent Progress on Urban Overheating and Heat Island Research. Integrated Assessment of the Energy, Environmental, Vulnerability and Health Impact Synergies with the Global Climate Change. *Energy and Buildings*, 207(1), 109482. 10.1016/j.enbuild.2019.109482

Schmidtlein, M. C., Deutsch, R. C., Piegorsch, W. W., & Cutter, S. L. (2008). A Sensitivity Analysis of the Social Vulnerability Index. *Risk Analysis*, 28(4), 1099–1114. https://doi.org/10.1111/j.1539-6924.2008.01072.x

Sharma, J., & Ravindranath, N. H. (2019). Applying IPCC 2014 framework for hazard-specific vulnerability assessment under climate change. *Environmental Research Communications*, 1(5). 10.1088/2515-7620/ab24ed

Shih, W.-Y., & Mabon, L. (2021). Understanding heat vulnerability in the subtropics: Insights from expert judgements. *International Journal of Disaster*

Risk Reduction, 63, 102463. https://doi.org/10.1016/j.ijdrr.2021.102463

Stewart, I. D., & Oke, T. R. (2012). Local climate zones for urban temperature studies. *Bulletin of the American Meteorological Society*, 93(12), 1879–1900. https://doi.org/10.1175/BAMS-D-11- 00019.1

Uejio, C. K., Wilhelmi, O. V., Golden, J. S., Mills, D. M., Gulino, S. P., & Samenow, J. P. (2011). Intra-urban societal vulnerability to extreme heat: The role of heat exposure and the built environment, socioeconomics, and neighborhood stability. *Health & Place*, 17(2), 498–507. 10.1016/j.healthplace.2010.12.005

Verdonck, M. -L., Demuzere, M., Hooyberghs, H., Beck, C., Cyrys, J., Schneider, A., Dewulf, R., & Van Coillie, F. (2018). The potential of local climate zones maps as a heat stress assessment tool, supported by simulated air temperature data. *Landscape and Urban Planning*, 178, 183–197. https://doi.org/10.1016/j.landurbplan.2018.06.004

Verdonck, M. L., Okujeni, A., van der Linden, S., Demuzere, M., De Wulf, R., & Van Coillie, F. (2017). Influence of neighbourhood information on 'Local Climate Zone'mapping in heterogeneous cities. *International Journal of Applied Earth Observation and Geoinformation*, 62, 102–113. 10.1016/j.jag.2017.05.017

Wehner, M., Stone, D., Krishnan, H., AchutaRao, K., & Castillo, F. (2016). The Deadly Combination of Heat and Humidity in India and Pakistan in Summer 2015. *Bulletin of the American Meteorological Society*, 97(12), 81–86. https://doi.org/10.1175/bams-d-16-0145.1

Wilhelmi, O. V., & Hayden, M. H (2010). Connecting people and place: a new framework for reducing urban vulnerability to extreme heat. *Environmental Research Letters*, 5(1), 014021. https://doi.org/10.1088/1748-9326/5/1/014021

Wolf, T., & McGregor, G. (2013). The development of a heat wave vulnerability index for London, United Kingdom. *Weather and Climate Extremes*, 1, 59–68. https://doi.org/10.1016/j.wace.2013.07.004

World Meteorological Organization. (2021). *State of the global climate 2020* (WMO-No. 1264). World Meteorological Organization. https://library.wmo.int/doc_num.php?explnum_id=10618

Wouters, H., De Ridder, K., Poelmans, L., Willems, P., Brouwers, J., Hosseinzadehtalaei, P., … & Demuzere, M. (2017). Heat stress increase under climate change twice as large in cities as in rural areas: A study for a densely populated midlatitude maritime region. *Geophysical Research Letters*, 44(17), 8997–9007. https://doi.org/10.1002/2017GL074889

Wu, J., Liu, C., & Wang, H. (2022). Analysis of Spatio-temporal patterns and related factors of thermal comfort in subtropical coastal cities based on local climate zones. *Building and Environment*, 207, 108568. https://doi.org/10.1016/j.buildenv.2021.108568

Zanter, K. (2016). *Landsat 8 data users handbook*. U.S. Geological Survey. https://landsat.usgs.gov/landsat-8-l8-data-users-handbook

Zhou, Y., Zhang, G., Jiang, L., Chen, X., Xie, T., Wei, Y., … & Lun, F. (2021). Mapping local climate zones and their associated heat risk issues in Beijing: Based on open data. *Sustainable Cities and Society*, 74(4), 103174. 10.1016/j.scs.2021.103174

Zou, Q., Yang, J., Zhang, Y., Bai, Y., & Wang, J. (2025). Variation in community heat vulnerability for Shenyang City under local climate zone perspective. *Building and Environment*, 267, 112242. https://doi.org/10.1016/j.buildenv.2024.112242

Zuhra, S. S., Tabinda, A. B., & Yasar, A. (2019). Appraisal of the heat vulnerability index in Punjab: a case study of spatial pattern for exposure, sensitivity, and adaptive capacity in megacity Lahore, Pakistan. *International Journal of Biometeorology*, 63(12). 10.1007/s00484-019-01784-0

Annexure I. Indicators of adaptive capacity, sensitivity and exposure

Variables	Indicators	Definition/method to quantify	Source
Adaptive Capacity (A_c)	1. Electricity supply (ES)	Ward-wise household per hectare that have electricity supply	Census of India-2011
	2. Water supply (WS)	Ward-wise household per hectare having water facility	
	3. Communication facilities (CF)	Ward-wise household per hectare that has landline and mobile phone	
	4. Health facilities (HF)	The distance of centroid of the continuous urban area in each ward to the nearest government hospitals	Remote Sensing & Nagpur Municipal Corporation
	5. Social facilities: religious facilities & schools (SF)	The distance of centroid of the continuous urban area in each ward to the nearest social facilities.	
	6. Personal vehicle (PV)	Ward-wise household per hectare having personal vehicle	Census of India-2011
	7. Bank account (BA)	Ward-wise household per hectare availing banking facilities	
	8. Normalized Difference Vegetation Index (NDVI)	An index for quantifying the health and density of vegetation	LANDSAT-8 imagery
Sensitivity (S)	9. Illiterate Population (IP)	Inhabitants per hectare who are illiterate	Census of India-2011
	10. Female population (FP)	Ward-wise female population per hectare	
	11. Population aged under 6 years (YP)	Inhabitants per hectare below six years age	
	12. Population aged over 60 years (OP)	Inhabitants per hectare with age equal to or greater than 60	
	13. Population of Scheduled Caste (SC)/Scheduled Tribe (ST)	Ward-wise population of SC/ST per hectare	
	14. Population density (PD)	Ward-wise population density per hectare	
	15. Typology of houses (TYP)	Ward-wise number of katcha/pucca houses per hectare	
	16. Single household size (SH)	Inhabitants per hectares who live alone	
	17. Average number of people per household (HH)	Ward-wise number of person per household	
	18. Rented housing (RH)	Ward-wise rented household per hectare	
	19. Roof material (RM)	Ward-wise household per hectare with roof material as asbestos/ metal/GI	
	20. Population with disability 18-64 years (DIS)	Ward-wise population that has disability 18-64 years	
Exposure (E)	21. Land Surface Temperature (LST)	An index which estimates radiative skin temperature of the land surface	LANDSAT-8 imagery

Annexure II. Ward-wise values for HVI

Name	Normalized values				
	adp_sc	exp_sc	sen_sc	hvi_total	hvi (out of 1)
WARD NO 1	0.626	0.461	0.339	1.426	0.484
WARD NO 2	0.463	0.555	0.471	1.489	0.512
WARD NO 3	0.115	0.426	0.363	0.905	0.255
WARD NO 4	0.130	0.338	0.680	1.147	0.361
WARD NO 5	0.102	0.626	1.000	1.728	0.617
WARD NO 6	0.041	0.665	0.866	1.572	0.548
WARD NO 7	0.631	0.092	0.255	0.979	0.287
WARD NO 8	0.431	0.091	0.176	0.698	0.164

Name	Normalized values				
	adp_sc	exp_sc	sen_sc	hvi_total	hvi (out of 1)
WARD NO 9	0.333	0.000	0.157	0.490	0.072
WARD NO 10	0.287	0.079	0.055	0.422	0.042
WARD NO 11	0.233	0.428	0.065	0.726	0.176
WARD NO 12	0.445	0.691	0.311	1.447	0.493
WARD NO 13	0.127	0.594	0.329	1.051	0.319
WARD NO 14	0.122	0.671	0.371	1.164	0.369
WARD NO 15	0.443	0.214	0.209	0.866	0.238
WARD NO 16	0.057	0.675	0.597	1.329	0.441
WARD NO 17	0.106	0.740	0.683	1.529	0.529
WARD NO 18	0.106	0.627	0.679	1.412	0.478
WARD NO 19	0.040	1.000	0.200	1.240	0.402
WARD NO 20	0.067	0.745	0.724	1.537	0.532
WARD NO 21	0.278	0.880	0.194	1.351	0.451
WARD NO 22	0.282	0.291	0.030	0.603	0.122
WARD NO 23	0.287	0.099	0.120	0.507	0.080
WARD NO 24	0.318	0.246	0.205	0.769	0.195
WARD NO 25	0.601	0.299	0.505	1.405	0.475
WARD NO 26	0.333	0.210	0.138	0.681	0.156
WARD NO 27	0.224	0.276	0.081	0.581	0.112
WARD NO 28	0.308	0.241	0.054	0.603	0.122
WARD NO 29	0.541	0.807	0.742	2.091	0.776
WARD NO 30	0.552	0.847	0.740	2.138	0.797
WARD NO 31	0.110	0.823	0.137	1.071	0.328
WARD NO 32	0.103	0.743	0.370	1.216	0.392
WARD NO 33	0.066	0.598	0.463	1.128	0.353
WARD NO 34	0.394	0.467	0.376	1.237	0.401
WARD NO 35	0.340	0.389	0.171	0.901	0.253
WARD NO 36	0.031	0.696	0.439	1.167	0.370
WARD NO 37	0.036	0.785	0.809	1.630	0.573
WARD NO 38	0.026	0.921	0.609	1.556	0.541
WARD NO 39	0.251	0.827	0.203	1.281	0.420
WARD NO 40	0.265	0.152	0.034	0.451	0.055
WARD NO 41	0.262	0.167	0.055	0.484	0.069
WARD NO 42	0.286	0.373	0.188	0.847	0.229
WARD NO 43	0.039	0.357	0.591	0.988	0.291
WARD NO 44	0.316	0.368	0.221	0.905	0.255
WARD NO 45	0.152	0.309	0.017	0.478	0.067
WARD NO 46	0.165	0.349	0.026	0.540	0.094
WARD NO 47	0.223	0.511	0.076	0.809	0.213
WARD NO 48	0.272	0.445	0.135	0.852	0.232
WARD NO 49	0.076	0.430	0.483	0.989	0.292
WARD NO 50	0.056	0.762	0.782	1.600	0.560
WARD NO 51	0.000	0.738	0.599	1.337	0.445

Name	Normalized values				
	adp_sc	exp_sc	sen_sc	hvi_total	hvi (out of 1)
WARD NO 52	0.509	0.243	0.204	0.955	0.277
WARD NO 53	0.649	0.283	0.358	1.290	0.424
WARD NO 54	0.606	0.430	0.380	1.416	0.480
WARD NO 55	0.435	0.510	0.305	1.250	0.407
WARD NO 56	0.649	0.709	0.615	1.972	0.724
WARD NO 57	0.588	0.442	0.613	1.643	0.579
WARD NO 58	0.320	0.545	0.201	1.065	0.325
WARD NO 59	0.504	0.617	0.332	1.453	0.496
WARD NO 60	0.306	0.465	0.000	0.771	0.196
WARD NO 61	0.286	0.511	0.014	0.811	0.213
WARD NO 62	0.396	0.237	0.031	0.664	0.149
WARD NO 63	0.265	0.409	0.023	0.697	0.163
WARD NO 64	0.330	0.441	0.177	0.948	0.273
WARD NO 65	0.340	0.213	0.445	0.999	0.296
WARD NO 66	0.659	0.355	0.500	1.513	0.522
WARD NO 67	0.125	0.496	0.722	1.344	0.448
WARD NO 68	0.568	0.315	0.163	1.046	0.317
WARD NO 69	0.353	0.434	0.183	0.970	0.283
WARD NO 70	0.219	0.201	0.260	0.679	0.155
WARD NO 71	0.272	0.448	0.263	0.983	0.289
WARD NO 72	0.076	0.447	0.261	0.784	0.202
WARD NO 73	0.056	0.446	0.259	0.761	0.191
WARD NO 74	0.000	0.446	0.257	0.703	0.166
WARD NO 75	0.509	0.445	0.255	1.209	0.388
WARD NO 76	0.649	0.444	0.253	1.346	0.449
WARD NO 77	0.606	0.444	0.251	1.301	0.429
WARD NO 78	0.435	0.443	0.248	1.126	0.352
WARD NO 79	0.649	0.443	0.246	1.338	0.445
WARD NO 80	0.588	0.442	0.244	1.274	0.417
WARD NO 81	0.320	0.441	0.242	1.003	0.298
WARD NO 82	0.504	0.441	0.240	1.185	0.378
WARD NO 83	0.306	0.440	0.238	0.984	0.289
WARD NO 84	0.286	0.439	0.236	0.961	0.280
WARD NO 85	0.396	0.439	0.234	1.068	0.327
WARD NO 86	0.265	0.438	0.232	0.934	0.268
WARD NO 87	0.330	0.437	0.229	0.996	0.295
WARD NO 88	0.340	0.437	0.227	1.004	0.298
WARD NO 89	0.659	0.436	0.225	1.320	0.437
WARD NO 90	0.125	0.435	0.223	0.784	0.201
WARD NO 91	0.568	0.435	0.221	1.224	0.395
WARD NO 92	0.353	0.434	0.219	1.006	0.299
WARD NO 93	0.219	0.433	0.217	0.869	0.239
WARD NO 94	0.272	0.433	0.215	0.920	0.261

Name	Normalized values				
	adp_sc	exp_sc	sen_sc	hvi_total	hvi (out of 1)
WARD NO 95	0.076	0.432	0.213	0.721	0.174
WARD NO 96	0.056	0.431	0.211	0.698	0.163
WARD NO 97	0.000	0.431	0.208	0.639	0.138
WARD NO 98	0.509	0.430	0.206	1.145	0.360
WARD NO 99	0.649	0.429	0.204	1.282	0.421
WARD NO 100	0.606	0.429	0.202	1.237	0.401
WARD NO 101	0.435	0.428	0.200	1.063	0.324
WARD NO 102	0.649	0.427	0.198	1.274	0.417
WARD NO 103	0.588	0.427	0.196	1.210	0.389
WARD NO 104	0.320	0.426	0.194	0.939	0.270
WARD NO 105	0.504	0.425	0.192	1.121	0.350
WARD NO 106	0.306	0.425	0.189	0.920	0.261
WARD NO 107	0.286	0.424	0.187	0.898	0.252
WARD NO 108	0.396	0.423	0.185	1.005	0.299
WARD NO 109	0.265	0.423	0.183	0.871	0.240
WARD NO 110	0.330	0.422	0.181	0.933	0.267
WARD NO 111	0.340	0.421	0.179	0.941	0.270
WARD NO 112	0.272	0.421	0.177	0.870	0.239
WARD NO 113	0.076	0.420	0.175	0.671	0.152
WARD NO 114	0.056	0.419	0.173	0.648	0.142
WARD NO 115	0.000	0.419	0.171	0.589	0.116
WARD NO 116	0.509	0.418	0.168	1.095	0.338
WARD NO 117	0.649	0.417	0.166	1.233	0.399
WARD NO 118	0.606	0.417	0.164	1.187	0.379
WARD NO 119	0.435	0.416	0.162	1.013	0.302
WARD NO 120	0.649	0.415	0.160	1.224	0.395
WARD NO 121	0.588	0.415	0.158	1.160	0.367
WARD NO 122	0.320	0.414	0.156	0.890	0.248
WARD NO 123	0.504	0.413	0.154	1.071	0.328
WARD NO 124	0.306	0.413	0.152	0.870	0.239
WARD NO 125	0.286	0.412	0.149	0.848	0.230
WARD NO 126	0.396	0.412	0.147	0.955	0.277
WARD NO 127	0.265	0.411	0.145	0.821	0.218
WARD NO 128	0.330	0.410	0.143	0.883	0.245
WARD NO 129	0.340	0.410	0.141	0.891	0.248
WARD NO 130	0.659	0.409	0.139	1.206	0.387
WARD NO 131	0.125	0.408	0.137	0.670	0.151
WARD NO 132	0.568	0.408	0.135	1.110	0.345
WARD NO 133	0.353	0.407	0.133	0.893	0.249
WARD NO 134	0.219	0.406	0.131	0.756	0.189
WARD NO 135	0.519	0.466	0.193	1.177	0.294
WARD NO 136	0.322	0.643	0.327	1.291	0.643